Masteroppgave

NTNU
Norges teknisk-naturvitenskapelige universitet
Fakultet for informasjonsteknologi og elektroteknikk
Institutt for elkrafteknikk

Amund Kulsrud Storruste

Method for prediction of frequency drop following large generator outages

Masteroppgave i Master of Energy and Environmental Engineering
Veileder: Kjetil Uhlen

August 2020

NTNU
Kunnskap for en bedre verden

Amund Kulsrud Storruste

Method for prediction of frequency drop following large generator outages

Masteroppgave i Master of Energy and Environmental Engineering
Veileder: Kjetil Uhlen
August 2020

Norges teknisk-naturvitenskapelige universitet
Fakultet for informasjonsteknologi og elektroteknikk
Institutt for elkraftteknikk

NTNU
Kunnskap for en bedre verden

Preface

This master's thesis concludes my degree Master of Science at the Norwegian University of Sciene and Technology (NTNU). I would like to thank Kjetil Uhlen for his guidance and supervision. I would also like to thank Kristoffer Halseth for his support throughout the project.

Trondheim, August 14, 2020.

Amund Kulsrud Storruste

Abstract

The near future energy system is expected to have a higher share of intermittent renewable energy sources and more distributed generation. This brings with it potential issues with regards to system stability in electrical transmission networks. By introducing a larger degree of controller interfaced generation the inertial properties of electrical power systems are diminished. Consequently, fault situations causing frequency deviations in the system will become harder to manage, with stricter time response demands for controllers. By simulating generator trips in the Nordic transmission system this project tests the accuracy of predicting the response of the system frequency of future disturbances through the use of aggregated turbine governor models, for the purpose of improving transmission system operators ability to accurately dimension availible primary reserves.

First, state-of-the-art of frequency control will be presented. This will be done by covering the different stages of frequency dynamics and control, and models for aggregating frequency system dynamics are presented. Then, the simulation software in terms of the PSSE Nordic 44 model and the ePHASORSIM real-time simulator will be covered. Additionally, a presentation on the development of aggregated turbine control will be presented. Finally, a case study will be completed for the the simulation and prediction of system frequency response. Four initial generator trips are simulated. Their frequency response is then used to tune the predictive transfer function models. Four new generator trips are then used to test the accuracy of the predictive transfer functions.

The frequency drop was predicted with an mean absolute error of 40 mHz and a mean absolute time deviation of 0.2 s. It is believed that the accuracy of predictions would improve given an inertia estimation process based on the initial rate of change of frequency of the case being predicted. Further work should tests should be performed for other values of system inertia based on available forecasts.

Sammendrag

Fremtidens elektriske kraftsystem er forventet å ha en høyere andel tidsvarierende fornybar energi og mer distribuert produksjon. Dette fører med seg potensielle utfordringer i forhold til systemstabiliteten i de elektriske transmisjonsnettene. Ved å introdusere en større andel produksjon med kraftelektronisk grensesnitt vil elektrisk inertia - eller treghet - og egenskapene som følger med det reduseres. Dette betyr at feil situasjoner som forårsaker frekvensavvik vil blir vanskeligere å håndtere, med mindre marginer for kontrollsystemene. Ved å simulere generatorutfall i det nordiske transmisjonssystemet forsøkes det i denne oppgaven å teste nøyaktigheten i å forutsi tidsresponsen for systemfrekvens for fremtidige forstyrrelser ved hjelp av aggregerte turbinkontrollere, med den hensikt å bidra til systemoperatørers mulighet til å bedre kunne dimensjonere tilgjengelige primærreserver.

Først, vi state-of-the-art frekvenskontroll bli presentert. Deretter vil forskjellige stadiene av frekvensdynamikken som følger generatorutfall bli gjennomgått, og generelle forenklede metoder for moddelering av kraftsystemer blir presentert. Så vil simuleringsprogramvaren og relevante modeller i form av PSSE Nordic 44 bus og sanntidssimulatoren ePHASORSIM introduseres. Til slutt vil casestudien gjennomført i denne oppgaven bli presentert. Fire initielle generatorutfall blir gjennomført. Disse brukes for å tilpasse modellvariablene i to prediksjonsmodeller. Fire nye generatorutfall gjennomføres så for å teste nøyaktigheten til prediksjonsmodellene.

Frekvensavvikene ble predikert med en gjenomsnittlig absolutt feil på 40 mHz og med en gjennomsnittlig absolutt tidsavvik på 0.2 s. Det er sannsynlig at nøyaktigheten til prediksjonene ville forbedret seg med en inertia estimering basert på den initielle endringsraten til frekvensen for hver testcase. Videre arbeid bør undersøke virkningen av endrede system inertia verdier basert på tilgjengelige prognoser.

Table of Contents

List of Figures

List of Tables

Abbreviations

WAMS	Wide Area Measurement Systems
WACS	Wide Area Control Systems
RoCoF	Rate of Change of Frequency
PMU	Phasor Measurement Unit
TSO	Transmission System Operator
FCR	Frequency Containment Reserves
LSE	Least Squares Estimation
WLSE	Weighted Least Squares Estimation
PV	Photovoltaics
AGC	Automatic Generation Control
FFR	Frequency Restoration Reserves
FMI	Functional Mock-up Interface
FMU	Functional Mock-up Unit
TDs	Transmission and Distribution systems
HVAC	High Voltage Alternating Current
HVDC	High Voltage Direct Current

Chapter 1

Introduction

Parts of this chapter are redrafts of [1].

1.1 Background and motivation / Background and objective

With the increasing share of renewable generation in the Nordic power system, traditional system inertia is decreasing [2]. Traditional power production in thermal, nuclear and hydro all use synchronous generators, which have their rotating masses coupled with the instantaneous frequency of the power system. Renewable generation sources such as wind and solar are instead connected to the grid through power electronic converter interfaces. Because of this they do not provide inertia to the system. This decrease in system inertia means that time margins for frequency control units becomes shorter, potentially resulting in larger frequency disturbances and a reduction in system stability.

Electrical system frequency drops if a generator is disconnected due to an unexpected fault. The power deficit that emerge from a generator disconnect is covered by drawing additional power from the systems connected synchronous generators. This additional power is taken from the kinetic energy of the rotating turbines, and a collective deceleration of the machine turbines occur. System frequency then drops due the coupling between machine speed and electrical frequency present in synchronous generators. The correlation between system inertia and frequency drops is illustrated in 1.1 where a typical system frequency following a generator disconnection is shown for different amounts of system inertia [3].

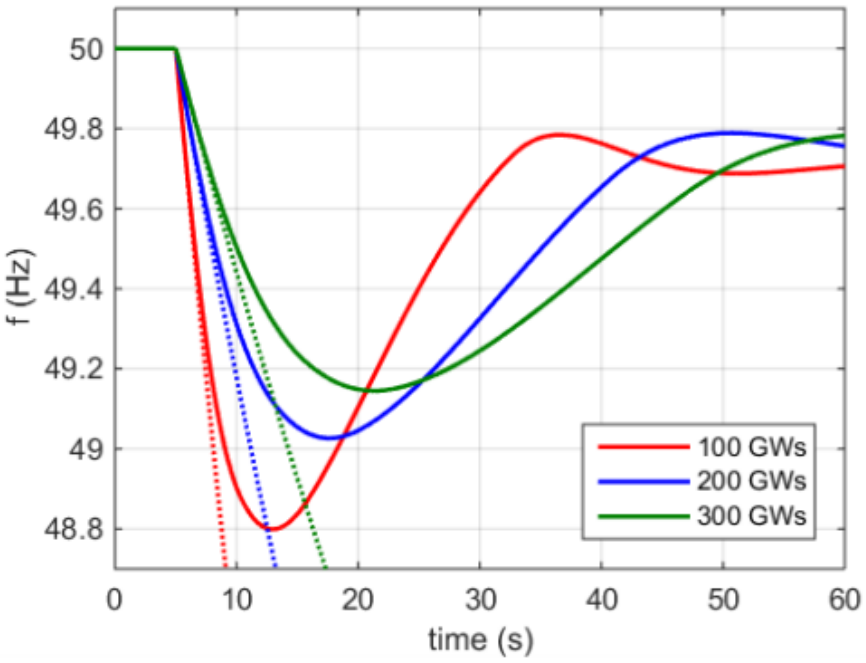

Figure 1.1: The typical time response of system frequency following a generator disconnect [3]. It is clear that the system inertia impacts the inital slope, the frequency drop, and swing time of the system. The steady state deviation does not depend on the system inertia and is therefore unchanged for the three cases.

Ultimately, the goal of frequency control is to contain the system frequency within an acceptable limit of the nominal system frequency, which in Europe is 50 Hz. The generating units participating in primary frequency control through automatic adjustment of generated power can be referred to as Frequency Containment Reserves (FCR). Statnett separates FCR into three categories as of 2019: normal operation (FCR-N), disturbance upwards regulation (FCR-D up), and disturbance downwards regulation (FCR-D down) [4]. The focus of this thesis will be on FCR-D upwards regulation following generator outages.

As the system frequency drops beneath 49.9 Hz FCR-D reserves are activated gradually until fully activated at 49.5 Hz, a 0.4 Hz range. Power input is increased and the initial Rate of Change of Freqency (RoCoF) of the system frequency is reduced. The maximum deviation in system frequency following the generator trip occurs a few seconds after the disturbance. We refer to the maximum deviation in system frequency as the *frequency drop*, denoted by Δf_{max}. The system frequency eventually stabilizes at a new steady state value, denoted by Δf_{∞}. The three quantities of initial RoCoF, frequency drop Δf_{max}, and steady state deviation Δf_{∞} describe the main impacts of a generator disconnect. The three quantities are indicated in figure 1.2 below.

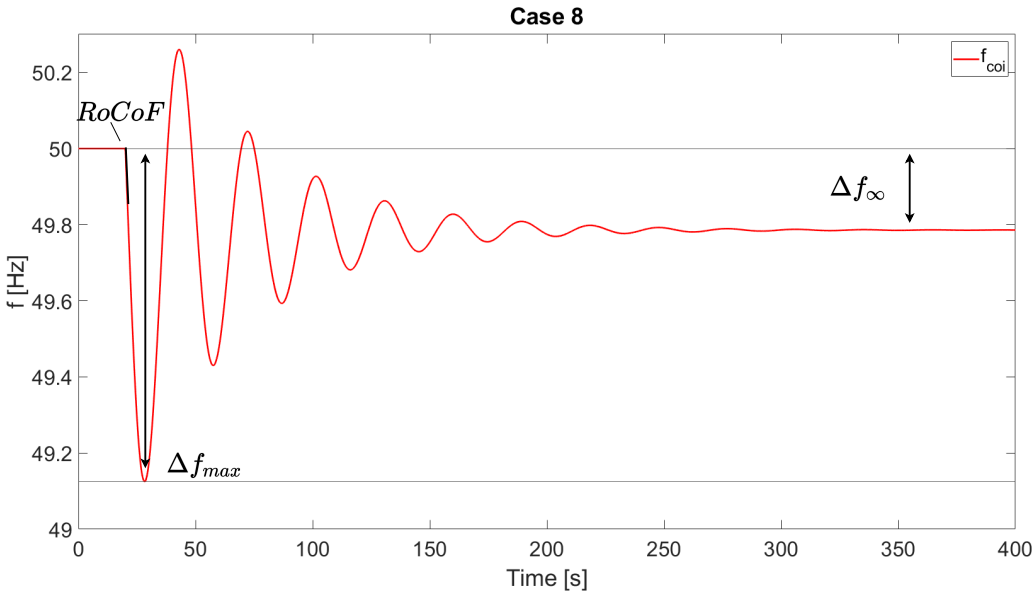

Figure 1.2: Illustration of important quantities for the response of the system frequency f_{coi} following a generator disconnection. The transient response can be described by the initial slope and Rate Of Change of Frequency (RoCoF), the initial frequency drop is indicated by the Δf_{max}, and the steady state deviation in system frequency is denoted as Δf_{∞}.

The reader is cautioned to distinguish between the terms system *frequency drop*, and system *droop*. The former, *frequency drop*, referring to the first nadir and minimum value of the system frequency following a generator disconnect. And the latter, system *droop*, is a property of the total FCR-D reserves defining the ratio between measured frequency and provided power, often denoted as ρ [Hz/MW]. Droop is the reciprocal of the effective gain of the system [5].

The potential frequency drop following generator disconnection is an important concern for Transmission System Operators (TSOs). The components connected to the system are specifically configured to operate at the rated system frequency, and too big of a deviation lasting too long will lead to disconnections. Automatic load shedding starts occurring at 48.8 Hz [6], which for normal operation is to be avoided. If the frequency drop continues even further, some generators may start disconnecting. The problem of stabilizing the system frequency is then further exacerbated. This could lead to cascading disconnections throughout the grid, and ultimately cause a complete blackout.

This thesis intends to assist TSOs in the process of predicting the magnitude of a frequency drop following potential future generator disconnections. Two predictive models are tested that can be used for estimating frequency drops. These predictive models are Laplace domain transfer functions developed from aggregated governor and system models. Each transfer function is tuned based on a previously simulated case, where the model representations of system inertia, governor gains, and governor time constants are chosen best on a best fit approach. The size of the power disturbance is assumed known and utilized in the process of tuning the transfer functions.

TSOs may use information about the transient frequency drop when determining what measures are needed to ensure system stability. The main available measures can be summarized as either increasing the kinetic energy of the system, increasing the aggressiveness or size of the FCR-D reserves, or supplementing FCR-D with controller interfaced power provision. In the Nordic synchronous area TSOs are planning to ensure future system stability through the latter option, by introducing a new Fast Frequency Reserve (FFR) [7]. The demand of the FFR reserve is going to be continuously evolving as the power system changes. This thesis is a contribution to the development of methods to quantify the need of FFR and other measures needed to ensure the stability of the elctrical transmission system.

1.2 Outline

The report is outlined as follows: In chapter 2 the reader is introduced with the theoretical framework relevant to this thesis. Chapter 3 presents the power system model and real time simulator used to imitate the behavior of a real transmission system. Afterwards relevant test and tune cases are summarized, and the process of tuning and testing the transfer function prediction models is explained. The results are presented in chapter 4 and then discussed in chapter 5. Finally conclusions and suggestions for further work is presented in chapter .

Chapter 2

Theory

This chapter is an introduction for the reader into the theoretical framework relevant to this thesis. Parts of this chapter are redrafts of [1].

First, an introduction to the frequency dynamics of individual synchronous generators is presented. Then the concepts for aggregating inertia and frequency are explained. Afterwards the control schemes and stage dynamics of frequency control is presented. Afterwards the concepts of Laplace transforms and block model representation are introduced, before finally deriving two system transfer functions from turbine governor models. Identification of relevant background material was carried out in the preceding specialization project. Part of this chapter is therefore a redraft of [1].

2.1 The swing equation

A synchronous generator transforms mechanical power into electrical power through a rotating turbine. The angular acceleration of the turbine can expressed from Newtons second law of rotation as:

$$J\vec{\alpha} = \vec{\tau}_{net} \tag{2.1}$$

Accelerating torque τ_m is provided by mechanical power applied to the turbine, typically as a stream of water or steam. Electrical power drawn from the machine provides turbine deceleration. A decelerating torque τ_e acts on the turbine through the magnetically coupled rotor- and stator field windings of the machine. This electromagnetic coupling synchronizes the mechanical speed of the turbine with the electrical frequency of the induced current at the machine terminals. Friction, magnetic losses, and damping is neglected. A simple illustration is shown in figure 2.1.

To express the rotor speed dynamics of a synchronous generator it is common practice to use equation (2.1) together with an inertial constant H[5]. This formulation is typically referred to as the *swing equation*. The inertial constant H is defined as the ratio $H =$

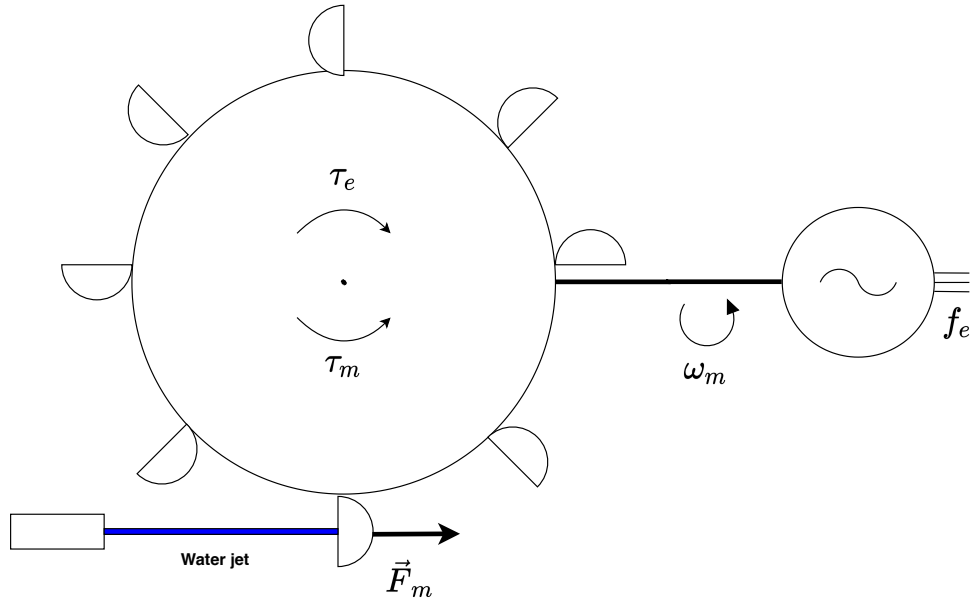

Figure 2.1: Simple sketch of how the mechanical torque τ_m and electrical torque τ_e work against each other to drive the mechanical speed ω_m of the rotating shaft of a Pelton wheel. Mechanical accelerating torque is developed from the force of the water jet $\vec{F}_m$. Electrical breaking torque is developed by the synchronous generator.

E_k/S_n, where E_k refers to the kinetic energy (J) of the turbine and S_n is machine rated power (W). The kinetic energy is referred to the turbine at rated speed ω_s such that $E_k = \frac{1}{2}J\omega_s^2$, which gives the following relationship for H:

$$H = \frac{\frac{1}{2}J\omega_s^2}{S_n} \quad [\text{s}] \tag{2.2}$$

The *swing equation* can then be expressed by combining equation (2.1) and (2.2) under the assumption that rotor speed is sufficiently close to rated speed:

$$2H\frac{\mathrm{d}\omega}{\mathrm{d}t} = \Delta P \tag{2.3}$$

where ω is rotor speed and ΔP is net power, both expressed in per unit values referred to rated speed ω_s and rated power S_n respectively. The net power can be calculated as the disparity between input mechanical power P_m delivered to the turbine shaft, and the electrical power P_e delivered to the power system at the generator terminals.

The Laplace transform of the swing equation can be useful. It is expressed in equation (2.4) below. The power system frequency Δf is used instead of the electrical angular speed $\Delta\omega$ of the machine rotor. This is possible due to the per unit values of system frequency and angular speed being identical for synchronous machines. Initial frequency deviation is assumed to be zero.

$$2Hs\Delta f = \Delta P \tag{2.4}$$

By expressing angular speed ω in terms of frequency f, the rate of change of frequency of any synchronous machine i connected to an electrical power system can be expressed as:

$$\frac{\mathrm{d}f_i}{\mathrm{d}t} = \frac{\Delta P_i}{2H_i S_{in}} f_n \quad [\mathrm{Hz/s}] \tag{2.5}$$

where ΔP_i is the disparity between input mechanical power and output electrical power (MW), f_i is electrical frequency (Hz), H_i machine specific inertia constant (s), S_{in} machine specific rated power (MVA), and f_n nominal system frequency (Hz)[8].

2.2 System inertia

The system dynamics can be approximated by aggregating all machines into a single synchronous generator. This assumes that individual rotor speed deviations are negligible. A power disturbance would then need to be shared, by connected synchronous generators, in such a way that equation (2.5) is fulfilled for a mutual $\frac{\mathrm{d}f}{\mathrm{d}t}$. Denoting the net power deviation as ΔP_{sys} and satisfying (2.5) gives the following expression for RoCoF for an aggregated system:

$$\frac{\mathrm{d}f}{\mathrm{d}t} = \frac{\Delta P_{sys}}{2\sum_{\forall\, i\in\mathcal{A}}(H_i S_{ni})} f_n \tag{2.6}$$

Here, the set of connected synchronous generators has been denoted by $\mathcal{A}$, and can be referred to as the active set. The total rated kinetic energy of the system is calculated as the sum $\sum H_i S_{ni}$, for all machines i part of the active set $\mathcal{A}$ (denoted as $\forall\, i \in \mathcal{A}$).

By introducing a system inertia constant H_{sys} it becomes possible to represent the system dynamics on a form similar to that of an individual synchronous machine. The *system inertia constant* H_{sys} represents the ratio between the total kinetic energy of the system, and total rated power of the system [9]. The system inertia H_{sys} is defined as in equation (2.7):

$$H_{sys} = \frac{\sum_{\forall\, i\in\mathcal{A}} H_i S_{in}}{\sum_{\forall\, i\in\mathcal{A}} S_{in}} \quad [\mathrm{s}] \tag{2.7}$$

Here H_i is the machine inertia and S_{in} is the rated power of each connected synchronous generator i. From this the *system swing equation* can be finally developed by combining equations (2.6) and (2.7):

$$\frac{\mathrm{d}f_{sys}}{\mathrm{d}t} = \frac{\Delta P_{sys}}{2H_{sys}S_{sys}} f_n \tag{2.8}$$

In equation (2.8) the net rated power of connected generators has been denoted by S_{sys}. The RoCoF represented by $\frac{\mathrm{d}f_{sys}}{\mathrm{d}t}$ is a system wide quantity shared by all connected generator. For a constant power disturbance experienced by a power system, the RoCoF calculated from (2.8) gives an aggregated frequency system response for all connected generators of the system. The reader should note that the frequency dynamics of each machine will be unique and oscillate around the system frequency. This is due to the imperfect distribution of electrical power contribution among connected generators during power disturbances[5]. Rotor swings are explained further in section 2.5.1.

For a short measurement period Δt following a power disparity ΔP, the system inertia constant H_{sys} can be estimated if the system frequency change Δf is measurable. For a 50 Hz system, this estimation becomes:

$$H_{sys} \approx \frac{\Delta P \cdot \Delta t}{\Delta f \cdot S_{sys}} \cdot 25 \tag{2.9}$$

2.3 Center of inertia frequency $\mathbf{f_{coi}}$

The center of inertia frequency f_{coi} is a way to aggregate the oscillatory response of many individual machines into a single quantity. It is a way of representing the system frequency response which takes into account the inertial contribution of each machine.

The weighted mean $\bar{x}$ of a set $\{x_1, x_2, \ldots, x_n\}$ with corresponding weights $\{w_1, w_2, \ldots, w_n\}$ can be defined as follows [10]:

$$\bar{x} = \frac{\sum_{i=1}^{n} w_i x_i}{\sum_{i=1}^{n} w_i} \tag{2.10}$$

Center of inertia frequency is a weighted mean of machine frequencies f_i where the weights are based on the rated kinetic energy $H_i S_{ni}$ of each respective machine i. Only the connected machines contributing electrical power during disturbances, represented by the active set $\mathcal{A}$, are included in f_{coi}. Based on this, the center of inertia frequency can be defined as [8]:

$$f_{coi}(t) = \frac{\sum_{\forall\, i \in \mathcal{A}} H_i S_{ni} f_i(t)}{\sum_{\forall\, i \in \mathcal{A}} H_i S_{ni}} \tag{2.11}$$

This effectively excludes frequency measurements at nodes with either no inertia H_i or no rated power S_{in} The expression can be simplified by normalizing the weights for each node i such that $w_i' = H_i S_{ni} / \sum_i^N H_i S_{ni}$ giving:

$$f_{coi} = \sum_{\forall\, i \in \mathcal{A}} w_i' f_i \tag{2.12}$$

2.4 Effective inertia

Controller interfaced generation does not contribute to system inertia by default. Provision of inertial frequency support is instead a configurable property. Wind power and solar photovoltaics (PV) are two examples of this. Modern wind power generation typically uses converter interfaced induction machines, which operate with turbine speeds different from synchronous speed. Solar PV uses DC to AC voltage source converters (VSCs) to provide power and has no rotating components. The power provided from both wind and solar PV generation sources are therefore, by default, unaffected by the power disparities experienced by their respective systems.

However, the power electronic surfaces also make the power provision configurable. This means that the inertial response of synchronous generators can be emulated. We refer to this as *synthetic inertia*. Implementation of synthetic inertia requires fast and accurate frequency measurements, and associated control schemes. As an example, the doubly-fed induction generator (DFIG) allows for adjustable power provision in wind power plants. The reader is referred to [11] by A. Storruste and O.M. Forbord for a thorough introduction on inertia emulation in wind powers systems.

To include the contribution of both synchronous and synthetic inertia, an effective inertia constant M can be introduced to represent the relationship between RoCoF and a power disparity. For synchronous machines the corresponding effective inertia constant can be derived from equation (2.5) as $M_i = \frac{2H_i S_{in}}{f_n}$. Like in section **??** power provision is assumed distributed such that local differences in RoCoF can be neglected. The effective inertia can then be used to express the immediate frequency dynamics following a load change in an area j:

$$\frac{\mathrm{d}f_j}{\mathrm{d}t} = \frac{\Delta P}{M_j} \tag{2.13}$$

where $\frac{\mathrm{d}f}{\mathrm{d}t}$ is the RoCoF, ΔP_j is the power deviation, M_j is the effective inertia, all referred to the system encompassed in area j.

2.5 Frequency dynamics

2.5.1 Stage I - Rotor Swings

For the first few seconds after a power disturbance, the individual dynamics of generators cause individual rotor swings in the system [5].

The power-angle relationship of a synchronous generator can be expressed on a simplified form as:

$$P_e = \frac{E'V}{X}\sin(\delta) \tag{2.14}$$

If there is a disconnection of a generator G_A, its equivalent impedance is also disconnected from the system. Seen from a separate generator G_B this correspond to the removal of a parallel impedance branch. Equivalent system impedance X seen from the separate generator G_B therefore drops. Consequently, from equation (2.14), it can be seen that the delivered power will drop proportionally. This is the immediate power drop from 1 to 2 illustrated in figure 2.2.

Input power P_m will then be larger than the output power P_e^-. The rotor will accelerate, until it reaches 4. At 4, rotor speed ω_m will be larger than synchronous speed ω_s, so the rotor angle δ will keep increasing. Input power P_m will then be less than output power P_e. Deceleration ensues. At point 3 the rotor is back at synchronous speed $\omega_m = \omega_s$, and so the rotor rate of change $\frac{\mathrm{d}\delta}{\mathrm{d}t}$ will be zero. Deceleration continues, and oscillations between the rotor angle and power at point 2 and 3 will occur. Damping and friction losses eventually cause the rotor angle and power to stabilize at 4.

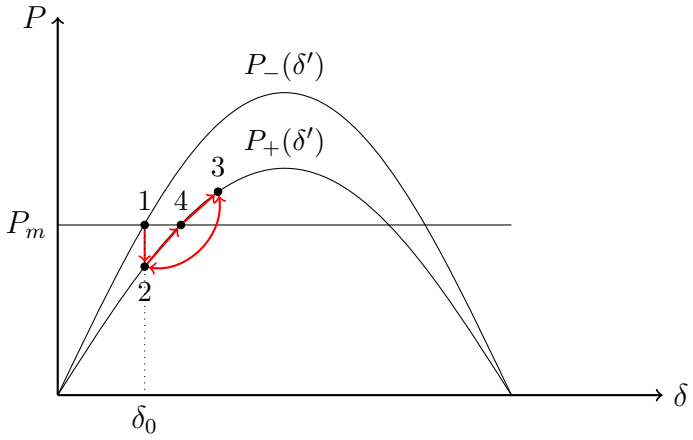

Figure 2.2: Rotor oscillations following an increase in impedance X.

2.5.2 Stage II - Frequency drop

After a few seconds of power imbalance, enough power has been taken from the rotating masses of the system to start slowing down. The system frequency drops, and the share at which each generator delivers energy depends on its inertial properties [5].

As the system frequency drops, all generator speeds ω_i will change at roughly the same rate [5]:

$$\frac{\mathrm{d}f_i}{\mathrm{d}t} \approx \varepsilon \quad , \quad \text{for all} \quad i \in N_G \tag{2.15}$$

Based on the assumption of a roughly shared system wide RoCoF stated in (2.15) , the individual power contribution ΔP_i of each machine can therefore be calculated from the swing equation in equation (2.5) as below:

$$\Delta P_i = \frac{2H_i S_{ni}}{f_n} \frac{\mathrm{d}f_i}{\mathrm{d}t} \tag{2.16}$$

It can be assumed from (2.15) that $\frac{\mathrm{d}f_i}{\mathrm{d}t} \approx \frac{\mathrm{d}f_{sys}}{\mathrm{d}t}$ for all synchronous generators connected to the system. Inserting equation (2.8), into (2.16) a final expressions for the power contribution of each individual generator is presented in equation (2.17) below. The expression indicates how much of the system wide disturbance ΔP_{sys} each connected synchronous generator must cover for the system to be changing at a shared RoCoF. This corresponds to the machine to system kinetic energy ratio E_i/E_{sys}, calculable from inertia and rated power coefficients H_i, S_{ni}, H_{sys}, and S_{sys}.

$$\Delta P_i = \frac{H_i S_{ni}}{H_{sys} S_{sys}} \Delta P_{sys} \tag{2.17}$$

2.5.3 Stage III - Primary response

During the third stage of the frequency response the Automatic Generation Control (AGC) is activated. AGC works to adjust the mechanical input power to match the output power. This is done at each generator through adjusting the physical valve controlling the input of typically steam or water. This control is implemented locally, so there is no communication needed between each generator. Rotor speed ω_m measurements are treated analogous to system frequency and are utilized as control input.

The specific behavior of a machine is described by the droop constant ρ, the machines rated power S_{ni}, and the nominal frequency of the system f_n in equation (2.18). Two alternative forms of the equation can be seen in (2.19)

$$\frac{\Delta f}{f_N} = -\rho_i \cdot \frac{\Delta P_i}{P_{ni}} \tag{2.18}$$

$$\Delta P_i = -\frac{P_{ni}}{\rho_i}\frac{\Delta f}{f_N} \Longleftrightarrow \left[\frac{\Delta P}{\Delta f}\right]_i = -\frac{1}{\rho_i}\frac{P_{ni}}{f_N} \tag{2.19}$$

From this, the total change of generated power ΔP_{tot} following a change in frequency is made up of the sum of all connected contributing generators:

$$\Delta P_{tot} = \sum_{i=1}^{N_g} \Delta P_i = \sum_{i=1}^{N_g} -\frac{P_{ni}}{\rho_i}\frac{\Delta f}{f_N} \tag{2.20}$$

The relationship between total change of generated power ΔP_{tot} and detected unit of change in frequency Δf can be expressed as $\left[\frac{\Delta P}{\Delta f}\right]_{sys}$, the frequency bias of the system. The experienced instantaneous change in frequency Δf is assumed to be the same for all connected generators. This holds true after the individual machine dynamics die out. The system frequency bias can then simply be found by summing up the frequency bias of each individual machine.

$$\left[\frac{\Delta P}{\Delta f}\right]_{sys} = \sum_{i=1}^{N_g} -\frac{1}{\rho_i}\frac{P_{ni}}{f_N} = \sum_{i=1}^{N_g} \left[\frac{\Delta P}{\Delta f}\right]_i \tag{2.21}$$

The frequency sensitivity of the system is the inverse of the frequency bias. After oscillations die out, the frequency sensitivity indicates the size of the steady state frequency deviation Δf_∞. Given a generator outage of a known size ΔP, the absolute value of the steady state frequency deviation can then be calculated from:

$$\Delta f_\infty = \frac{\Delta P}{\left[\frac{\Delta P}{\Delta f}\right]_{sys}} \tag{2.22}$$

In Norway the primary response is split into two, FCR-N and FCR-D, respectively for normal operation and disturbances. Normal operation is considered in a frequency range of ± 0.1 Hz from nominal, whereas distribution-range is considered as $49,9 - 49,5$Hz with full activation at 49.5 Hz [12].

2.5.4 Stage IV - Secondary response

After the primary response has stabilized the frequency there will be a constant frequency deviation. The secondary response consists of frequency restoration reserves that slowly bring the frequency back to its nominal value. The reader is referred to [13] for more on secondary frequency control schemes.

2.6 Laplace transforms

The laplace transform can be used to assess a time varying signal. By applying the laplace transform to a time varying signal, the corresponding laplace transform is produced. In particular, due to the swing equation being a differential equation, laplace helps simplifying the analysis of the system. The laplace transform $F(s)$ is a frequency dependant function. The variable s denotes the Laplace operator and can be interpreted as the frequency of a time varying signal. The following definition is used for the Laplace transform:

$$F(s) = \mathcal{L}\{f(s)\} = \lim_{\tau \to \infty} \int_0^\tau e^{-st} f(t) dt \tag{2.23}$$

The laplace transform of a derivate makes it so that

$$2H \frac{\mathrm{d}\omega}{\mathrm{d}dt} = \Delta P \tag{2.24}$$

$$2Hs\omega = \Delta P \tag{2.25}$$

This is easier to solve. We express the regulators, P, PI, and PID in the same way and then we transform back.

The unit step functing becomes the follwing with regards to laplace

$$\mathcal{L}\{u(t)\} = \frac{1}{s} \tag{2.26}$$

Unit step power disturbances ΔP can therefore be treated through its laplace transform $\frac{\Delta P}{s}$.

2.7 Block diagrams

The following section is described in [14]. The transfer function is referred to as $g(s)$, since the letter H refers to system inertia.

If initial conditions are zero, the behavior of a linear system can be described through its transfer function and input. The transfer function $g(s)$ can be expressed as a fraction of the output $y(s)$ by the input $u(s)$.

$$g(s) = \frac{y(s)}{u(s)} \tag{2.27}$$

For a feedback loop a simplification to the block diagram can be made to express the system in a single transfer function. This is suitable when modelling the feedback behavior of the frequency primary control mechanism of electrical power systems. The generalized transfer function for forward transfer function $h_1(s)$, and a function $h_2(s)$ in the feedback loop results in the following expression:

$$\frac{y(s)}{u(s)} = \frac{h_1(s)}{1 + h_1(s)h_2(s)} \tag{2.28}$$

This general concept is illustrated in the figure below.

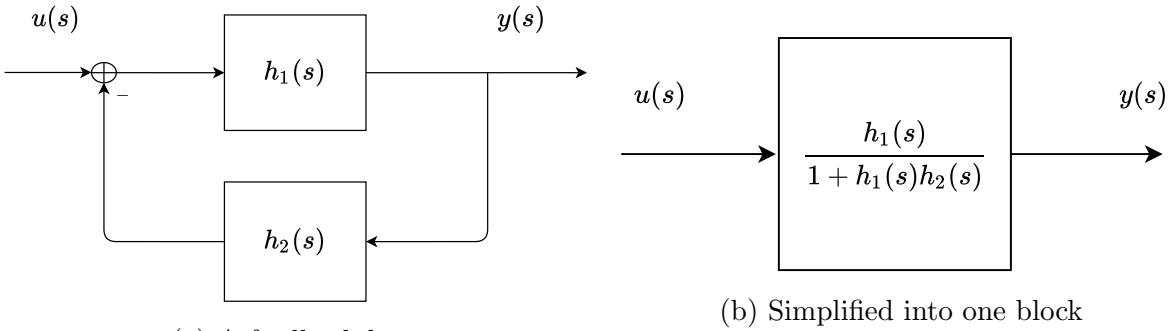

(a) A feedback loop

(b) Simplified into one block

Figure 2.3: Block diagram feedback loop

2.8 System transfer functions

The theoretical background for the modelling of the frequency control of an electrical power system is presented in this section. Two controller models are presented. Each controller model is ultimately represented by the system transfer functions $G_1(s)$ and $G_2(s)$. These transfer functions take a power disturbance P_d as their input and returns a system frequency deviation Δf as their output. $G_1(s)$ represents turbine governors with proportional (P) control, while $G_2(s)$ represent a proportional-integral (PI) control. The two models effectively represent turbine control with and without transient droop. In [15] the similarity between PI-regulation and transient droop compensation is shown.

The theory is mostly expressed in the Laplace domain, where the variable s is used to denote the Laplace operator.

2.8.1 Servomotor model

Before developing expressions for system frequency control, a general expression for the mechanical control system must be developed. The driving power of synchronous machine generation plants come from the mass flow driving the turbine rotor. This can be in the form of wind, gass flow, or for hydro power plants typical in Norway, water flow. To control the mass flow, flow gates controlled by a valve which can be opened or closed. The gate position can be indicated as g and is a range from 0 to 1. A change in gate position is referred to as Δg. Servomotors are used to control the position of the gate, and the signal input to the motor is referred to as the gate signal c. A change in the gate signal

is referred to as Δc.

Changing of gate positions allows the controller to adjust the mass flow interacting with the generator turbines, ultimately controlling the mechanical driving power P_t. The dynamics of the water flow in the turbines was not considered within the scope of the thesis. Therefore these dynamics have been neglected, and are not included in the following system aggregations. Instead the turbine power P_t is considered directly controllable by gate position g.

A general model for a servomotor can be expressed as in figure 2.4 below[5]:

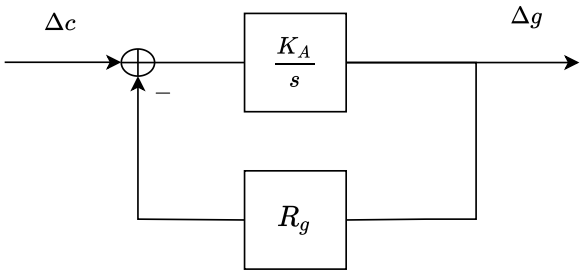

Figure 2.4: Control loop model of the servomotor of a turbine governor.

Here the servomotor is modelled as an integrator with a negative feedback loop. K_A is the forwards amplification gain, while the R_g corresponds to the gain in the feedback loop. Simplifying the control loop into a single block can be done, and the corresponding servomotor block becomes as shown in the expression below.

$$\frac{\Delta g}{\Delta c}(s) = -\frac{K_g}{T_g s + 1} \tag{2.29}$$

where, the servomotor gain is defined as $K_g = \frac{1}{R_g}$, and the servomotor time constant is defined as $T_g = \frac{1}{K_A R_g}$.

2.8.2 First order turbine governor

To construct a simple proportional controller a proportional gain block K_p is connected in series with the servomotor, shown in figure 2.5.

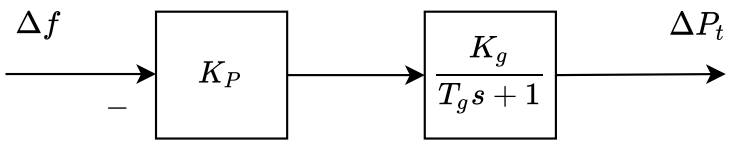

Figure 2.5: A simple proportional gain is used to control the servomotor controlling turbine power in a generator. The model can be used to develop a simple expression for the primary turbine response of an electrical power system.

The electrical frequency is used instead of rotor speed, due to the two being identical in terms of per unit values for synchronous machines[16]. The turbine mechanical power is assumed directly controllable from gate position, neglecting water flow dynamics. Change in gate position Δg is therefore replaced by ΔP_t. The total gain $K = K_p K_g$ can be considered the inverse what is typically referred to as governor droop. The turbine governor transfer function is expressed in equation (2.30).

$$G_P(s) = \frac{\Delta P_t}{\Delta f}(s) = -\frac{K}{Ts + 1} \tag{2.30}$$

It should be noted that this turbine governor representation is very basic. It is able to give a negative proportional response to a step disturbance, and approaches the steady state solution of a more complicated governor turbine model. But because of the simplifications, much of the dynamic behaviour is lost. Transient droop (similar to an integrator branch in a PI-controller) has been completely excluded, and the water dynamics have also been neglected. Nevertheless, this is a simple representation that is easily implemented for simulations.

The system transfer function $G_1(s)$ is developed by combining the swing equation with the simple proportional governor control in the previous section. An illustration of how the blocks interact is shown in figure 2.6. The system transfer function $G_1(s)$ from disturbance P_d to system frequency Δf can then be expressed as the following second order transfer function below. Two possible, but equivalent, formulations are presented in (2.31).

$$G_1(s) = \frac{\Delta f}{P_d}(s) = \frac{Ts + 1}{2HTs^2 + 2Hs + K} = \frac{\frac{1}{2H}s + \frac{1}{2HT}}{s^2 + \frac{1}{T}s + \frac{K}{2HT}} \tag{2.31}$$

Three parameters make up $G_1(s)$. The inertia H, the governor gain K, and the governor time constant T. The parameters can be determined from the rated values of their machines.

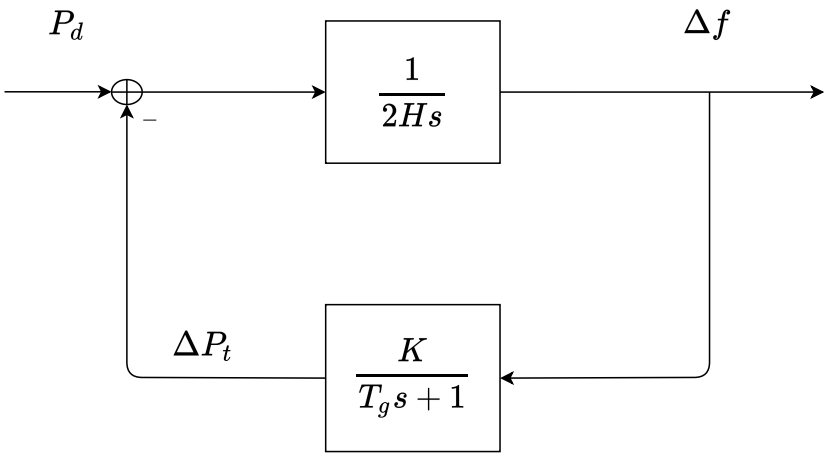

Figure 2.6: Illustration of the power system interactions of a synchronous generator with a first order turbine governor function. The setup represents the behavior of a single machine, but can also be used to describe the aggregated dynamics of a larger power system.

2.8.3 Second order turbine governor

The system transfer function $G_2(s)$ is developed by including a proportional-integral (PI) controller in the turbine governor model. This allows for the governor to be represented by a 2nd order transfer function $G_{gov}(s)$, which in turn makes the system transfer function $G_2(s)$ into a 3rd order transfer function.

The PI-controller can be expressed by supplementing the proportional gain K_P in figure 2.5 with a parallel integrator branch $\frac{K_I}{s}$ and a negative feedback loop. The gate signal Δc is in this model fed back through a permanent droop R_p and subtracted from the system frequency deviation Δf.

It can be noted that a transient loop feedback provides the same control advantages as a PI-controller. The transient loop feedback is an alternative modelling scheme. For this alternative scheme, a feedback loop with a frequency depended droop gain R_t is used, instead of the forward PI block. Both PI-control and transient droop feedback ensures the governor has a small gain for fast deviations in frequency, while keeping the gain high during steady state operation[15]. We refer to this as transient droop increase. Transient droop governor models can be found in [15] and [5]. A model similar to the PI-controller in figure 2.7a can be found in the PSSE Nordic 44 system in the HYGOV turbine governor[17]. See section 3.4 for more on this HYGOV model. Block diagrams for a PI-controller and a transient droop feedback loop are presented in the figure below:

The pilot servomotor dynamics have been neglected in both 2.7a and 2.7b due to it's time constant being significantly smaller than the other system parameters. The pa-

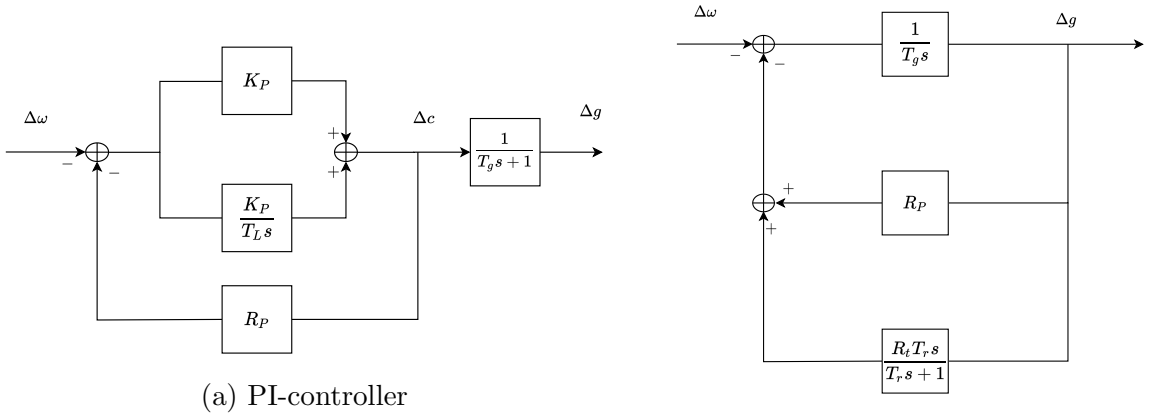

(a) PI-controller

(b) Transient droop

Figure 2.7: Two different modelling approaches for hydraulic turbine governors, with (a) PI-controller, and (b) transient droop. The two models both allow for a reduced gain for fast disturbances and a high gain for steady state. The PI-controller uses the gate signal Δc as feedback, while the transient droop model uses the gate position Δg.

rameters in the PI-controller consist of proportional gain K_P, integral time constant T_L, permanent droop R_P, and servomotor time constant T_g. Some of the same parameters also appear in the transient droop model. Both models may be expressed through the generalized transfer function:

$$\frac{\Delta g}{\Delta \omega}(s) = K \frac{T_1 s + 1}{(T_2 s + 1)(T_3 s + 1)} \tag{2.32}$$

For the PI-controller one can show that $K = \frac{1}{R_P}$, $T_1 = T_L$, $T_2 = \frac{T_L}{K_P R_P} + T_L$, and $T_3 = T_g$. The reader is referred to [5] for how the transient droop model can be expressed from (2.32).

The system model $G_2(s)$ can now be developed by again considering the full system as an aggregated single synchronous generator from (2.4), and an aggregated turbine governor from (2.32). The mechanical power P_t is assumed directly controllable from the gate Δg, by neglecting water dynamics, and turbine speed $\Delta\omega$ is expressed as system frequency Δf. This allows expressing the governor transfer function $G_P I(s)$ in equation (2.33), and the corresponding aggregated power system is shown in figure 2.8.

$$G_{PI}(s) = \frac{\Delta P_t}{\Delta f} = K \frac{T_1 s + 1}{(T_2 s + 1)(T_3 s + 1)} \tag{2.33}$$

Finally the system transfer function $G_2(s) = \frac{\Delta f}{P_d}$ is found by eliminating the feedback loop for primary response. This system transfer function has been formulated in two ways in the equation below:

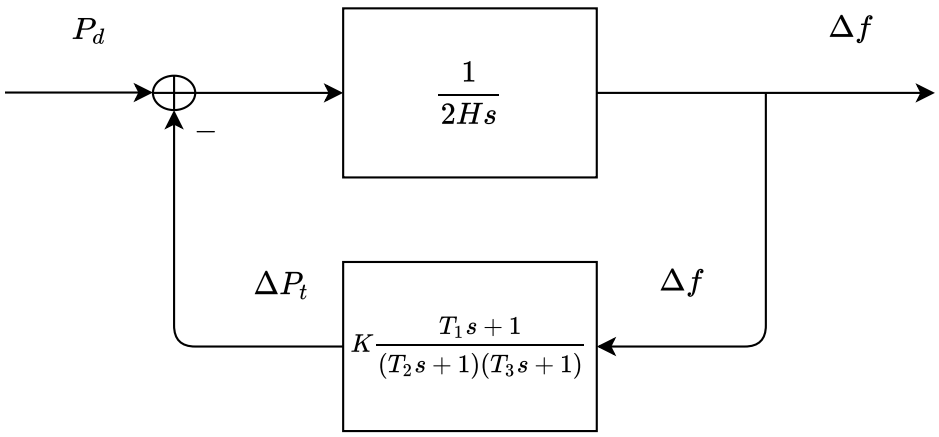

Figure 2.8: Block diagram of system with PI-controlled turbine governors on simplified form.

$$G_2(s) = \frac{\frac{1}{2H}s^2 + \frac{T_2+T_3}{2HT_2T_3}s + \frac{1}{2HT_2T_3}}{s^3 + \frac{T_2+T_3}{T_2T_3}s^2 + \frac{2H+KT_1}{2HT_2T_3}s + \frac{K}{2HT_2T_3}} \tag{2.34}$$

2.9 Tuning of K from steady state frequency deviation

The steady state frequency deviation for both system transfer functions $G_1(s)$ and $G_2(s)$ can be shown to correspond with the primary response mechanism presented in section 2.5.3. To show this the Final Value Theorem (FVT) is applied on both $G_1(s)$ and $G_2(s)$. FVT can be defined as below[18]:

$$y(t \to \infty) = \lim_{s \to 0} sY(s) \tag{2.35}$$

Here, $Y(s)$ is the Laplace transformation of the function $y(t)$, and s is the Laplace domain operator.

A unit step disturbance $P_d(s) = \frac{P_d}{s}$ is considered as the system input. The frequency deviation is expressed in (2.36) from the system transfer functions and unit step disturbance, all in their respective Laplace transformations. The transfer functions are denoted as $G_i(s)$ for $i \in [1, 2]$.

$$\Delta f(s) = G_i(s)P_d(s) = G_i(s)\frac{P_d}{s} \tag{2.36}$$

By applying the FVT to equation (2.36) the steady state frequency deviation is expressed in equation (2.37) below.

$$\Delta f(t \to \infty) = \lim_{s \to 0} G_i(s)P_d = \frac{1}{K}P_d \tag{2.37}$$

By comparing (2.37) to (2.22) it becomes apparent that K approaches the primary response system bias $\left[\frac{\Delta P}{\Delta f}\right]_{sys}$ for both $G_1(s)$ and $G_2(s)$.

Based on equation (2.37) a method for tuning the K parameter is developed. For each respective tuning case presented in 3.4.1, the active power disturbance is divided by the measured frequency deviation 400 seconds into the performed simulation. This is finally summarized in equation (2.38) below:

$$K = \frac{P_d}{\Delta f(t = 400)} \tag{2.38}$$

Chapter 3

Method

3.1 Simulator and model

Power system simulations allows for many opportunities when developing the control systems of tomorrow. Simulating the power system allows for the possibility of configuring the system for different situations. Different shares of type of generation may be constructed scenarios. The location of load and its sensitivity to factors like frequency and voltage may be tuned. Different control systems and controllers may be tested for different situations. In short a lot of opportunities for experimentation is made possible by the use of simulation software. Additionally, with how crucial electric distribution is to both industry and the everyday life of people, the ability to experiment directly on the system is very limited. By utilizing simulations, these issues can be bypassed and thorough analysis may performed without affecting connected users.

Being able to run real-time simulations is also a great advantage. This way experience and time aspects of faults can also be experienced. It is then possible to get a first hand impression of how a system response would look to an operator. Control schemes activated at different times may perform differently, and having the freedom to make control choice in real-time would give a sense of the urgency and consequences of actions.

3.2 Nordic 44 test network

The model used in the case study is the PSSE version of the Nordic-44 bus model (N44). This is a PSSE configuration that covers the Nordic area consisting of Norway, Sweden, Åland, Finland, and northern Denmark. The responsible transmission system operators (TSOs) are respectively Statnett, Svenska kraftnät, Kraftnät Åland, Fingrid, and Energinet. System operation agreements exists, requiring a common effort to secure reliable operation of high quality throughout the interconnected nordic power system [19].

An illustration of the Nordic transmission network is shown in figure 3.1. In 3.1a to the left, the Nord Pool bidding zones are illustrated as of 2015 [13]. In 3.1b on the right the Nordic 44-bus (N44) test network used in this thesis is presented. The N44 test network is an aggregated representation of the Nordic transmission system, with generation, load, and transmission lines. Peripheral areas such as UK, Germany and the Baltic states are represented by connecting loads. The Nord Pool bidding zones map can be used as an approximate visual representation of the area covered by the N44 model.

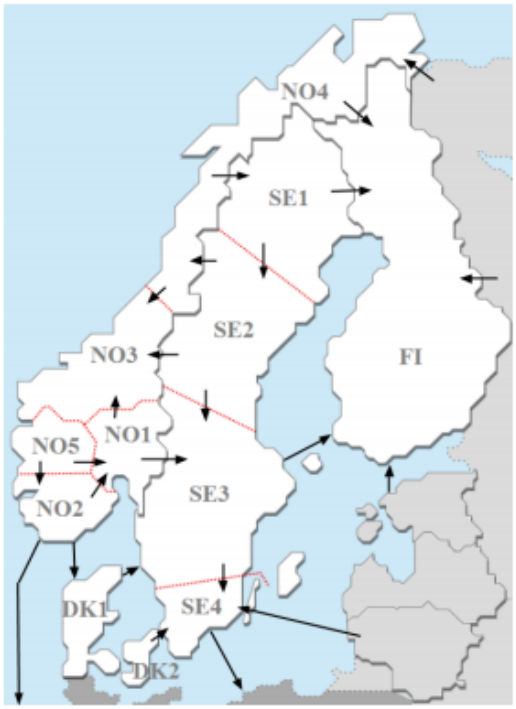

(a) Nord Pool bidding zones from 2015 [13].

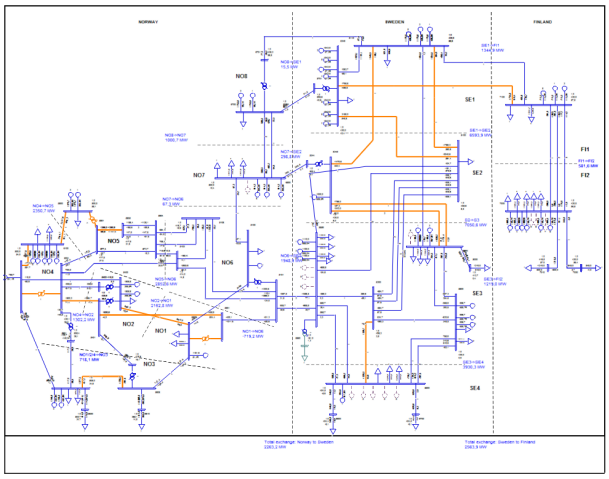

(b) N44 PSSE single line diagram.

Figure 3.1: Illustration of interconnected nordic network alongside the N44 test network representation of the same grid.

The N44 model has been developed at The Norwegian University of Science and Techonology (NTNU) and has gone through many different iterations over the years [20]. The N44 PSSE version provided by Tor Inge Reistad has been used, which is the same version as in [21] developed by Dinh Thuc Duong. In total the system consists of 44 buses, 18 power plants represented by 61 machines, 43 loads, 67 transmission lines, altogether representing the 320 kV and 400 kV voltage levels of the nordic synchronous area.

3.3 ePHASORsim

ePHASORSIM is a simulation software engine developed by OPAL-RT Technologies. The software is capable of simulating the real-time dynamics of large-scale transmission and distribution power systems. According to [22] it is able to simulate models with over 108 000 nodes.

The ePHASORSIM software is accessed through a solver block in Simulink. This block is able to simulate the specified PSSE model file in real time inside the simulink environment. Because of this MATLAB was chosen as the programming interface used for handling the prediction methods developed in this thesis. It was thought that online control applications could more easily be implemented back into Simulink if MATLAB was used. No such online applications were developed in the end. MATLAB was nevertheless a practical choice due to the simplicity of storing and using the measured data.

To configure the outputs and inputs taken from system, an excel file accessed by the solver block is made. ePHASORSIM has built in specific codes for how this is done. Measures for bus voltage, line currents, and rotor speeds are examples of states that can be read out and updated continuously throughout a simulation. In the case of frequency, measurements of generator rotor speed can be converted into local frequency. Many possible inputs are also possible, such as tripping a bus or initiating a three-phase-to-ground fault on a line.

The interactions between the inputs and outputs, and the real time system simulations are kept in separate subsystems. A master block is used for the solver block sending its system outputs to the control block. The control block stores the measured data sent from the solver, and signals for disconnecting generator and potentially changing system parameters are configured here. Communication blocks are used to relay signals from one block to the other. The Simulink setup is illustrated in figures 3.2, 3.3, and 3.4 below.

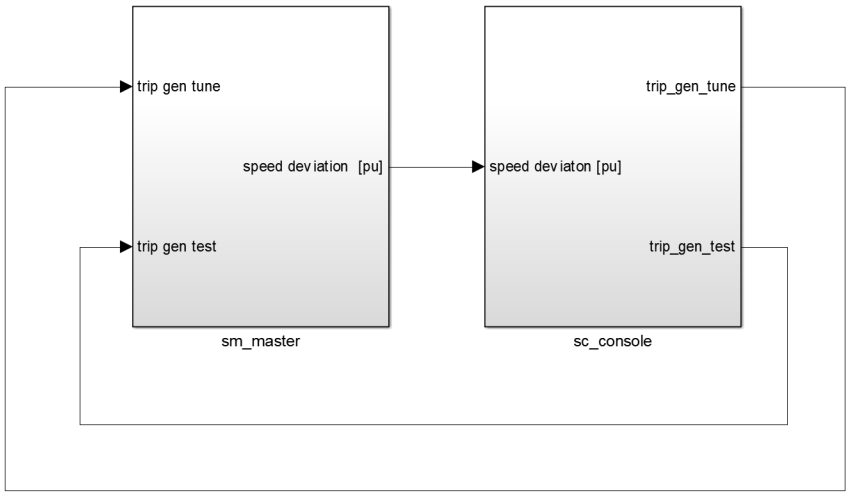

Figure 3.2: Simulink block setup illustrating the two subsystem for simulation and control.

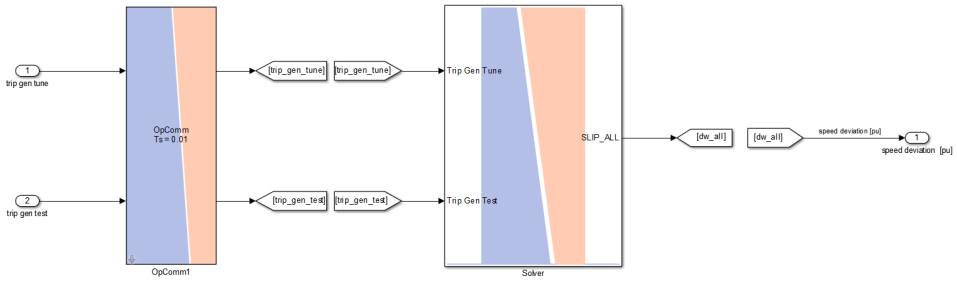

Figure 3.3: Simulation subsystem block leading the generator disconnect signal through a communications block into the solver block. The solver block then outputs the turbine speed deviations in per unit.

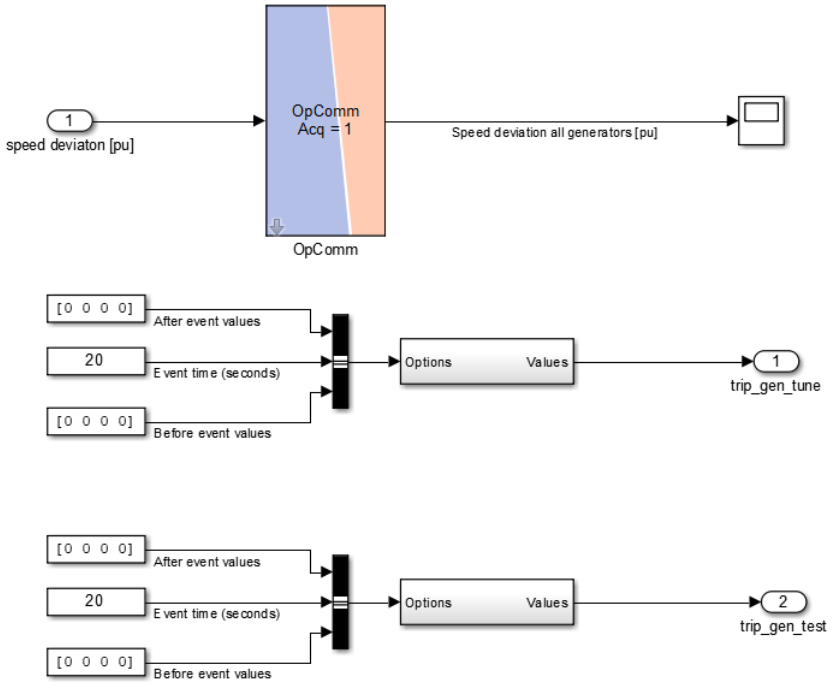

Figure 3.4: Control subsystem block taking the turbine speed deviations through a communications block and storing the measurements to the MATLAB workspace through a scope block. Below is the switches used for disconnecting one of the specified generators of the N44 PSSE model.

3.4 PSSE HYGOV model

The turbine governor model responsible for primary control in the PSSE N44 model is the HYGOV generator. It's specifications can be found in [17]. Its block diagram from PSSE documentation is presented below.

One can recognize several key control parameters in PSSE model shown in 3.5. Turbine speed deviation $\Delta\omega$ is used as input. The controller consists of a filter $\frac{1}{1+T_f s}$, a transient droop block $\frac{1+T_r s}{rT_r s}$, and feedback loop with droop R. This results in a gate signal c which through a servomotor block produces the gate position g. The gate position interacts with the waterway dynamics through the water time constant T_w. Mechanical power is finally expressed as the output of the model. The key model is summarized on a more compact format below:

Simplifying the HYGOV-model further can by done by neglecting the filter and water dynamics blocks. The filter time constant is necessary to eliminate high frequency noise

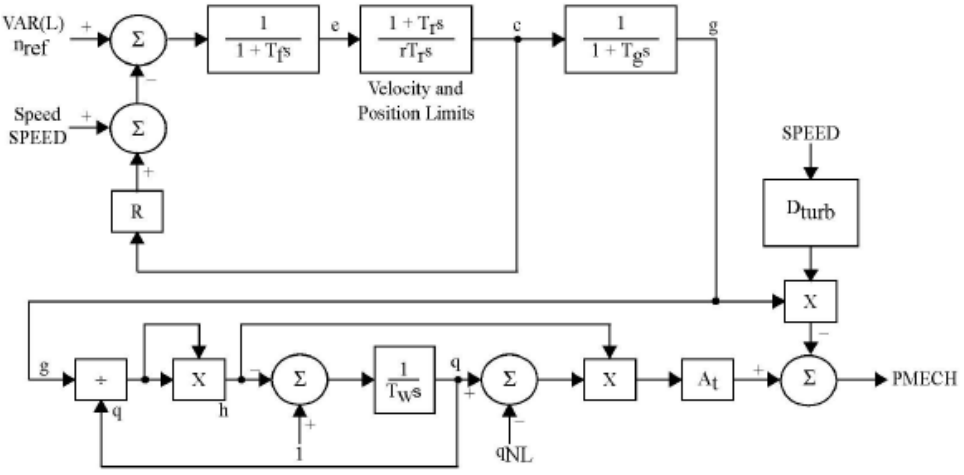

Figure 3.5: PSSE model description of the HYGOV model simulating a typical turbine governor in a hydro power plant[17]. The model can be seen to take turbine speed (SPEED) as its input and returning mechanical power (PMECH). The top part of the diagram represents the controller, while the bottom part represents the dynamic response of the water flow.

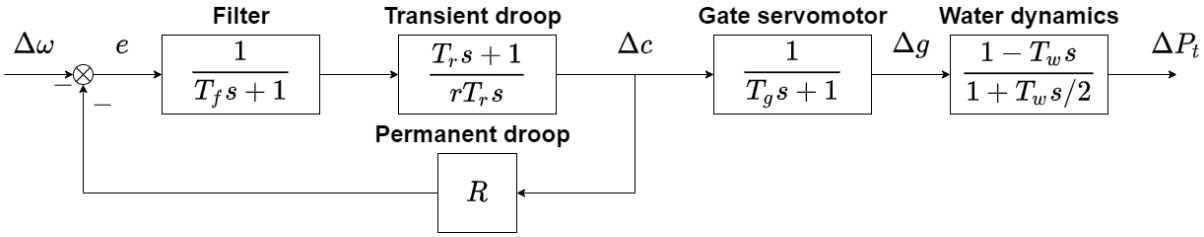

Figure 3.6: A summary of the key blocks in the HYGOV PSSE model and what they represent. Included are indicators for speed deviation $\Delta\omega$, change in gate signal Δc, change in gate position Δg, and ultimately change in mechanical turbine power ΔP_t.

in the input. This is not an issue in a simulated environment and so the filter block is disregarded. The water dynamics are present in the system modelling, but is outside the scope of this thesis and is therefore also disregarded. This leaves a more concise turbine generator block summarized by a permanent droop, transient droop, and a gate servomotor. The block diagram is shown in figure 3.7.

The controller in this expression is on the same form as a PI-controller would look. This becomes apparent through some manipulation of the transient droop block in the forward loop. By choosing $K_P = \frac{1}{r}$ as the proportional gain, and $K_I = \frac{1}{rT_r}$ as the integral gain, one gets a traditional formulation of a PI-controller in $\frac{T_r s+1}{rT_r s} = K_P + \frac{K_I}{s}$. An equivalent model could then be expressed as in figure 3.8 below:

The turbine governor transfer function encompassing the elements of the simplified

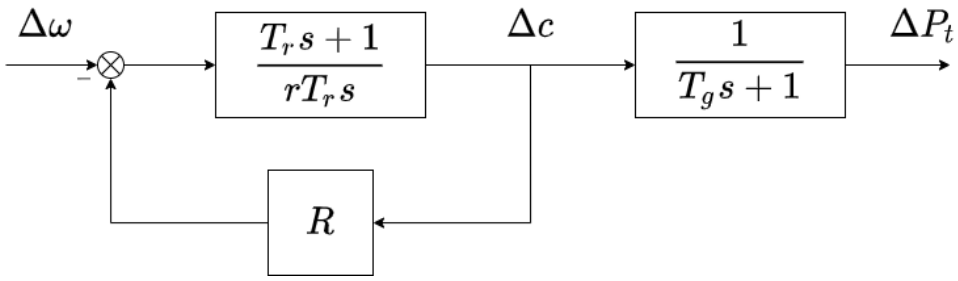

Figure 3.7: Simplified version of the HYGOV PSSE model. The filter and water dynamics blocks have been neglected and only the permanent droop block, transient droop block, and gate servomotor block is left.

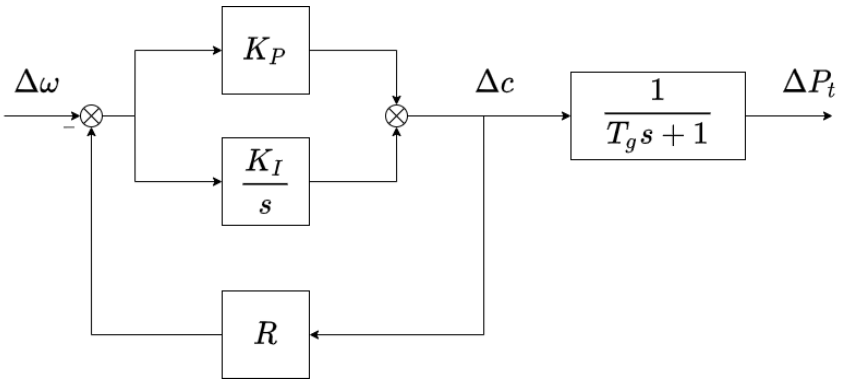

Figure 3.8: An alternative for of the PSSE model where the transient droop block has been replaced by a proportional gain K_P and integral gain K_I. The ultimate governor function would be the same, and so the two formulations are interchangeable from a system point of view.

HYGOV-model can be expressed as in the following equation:

$$\frac{\Delta P_t}{\Delta \omega}(s) = \frac{1}{R} \frac{T_r s + 1}{(\frac{r}{R} T_r + T_r)s + 1} \frac{1}{T_g s + 1} \tag{3.1}$$

A generalized transfer function representing a single HYGOV turbine governor model from the PSSE model can therefore be expressed as:

$$G_{gov}(s) = K \frac{T_1 s + 1}{(T_2 s + 1)(T_3 s + 1)} \tag{3.2}$$

where, $K = 1/R$, $T_1 = T_r$, $T_2 = \frac{r}{R} T_r + T_r$, and $T_3 = T_g$.

3.4.1 Cases

Eight different cases were introduced where different generators were disconnected from the system model. The chosen generators are representations of generators existing in real life. Oslo 2 is the exception to this, as the model is an aggregated representation of a large amount of smaller generation sources. It was nevertheless included on the basis that this hypothetical generator disconnect provided a valuable diversification of the test cases. In table 3.1below the specifications for the 8 cases are presented, and their geographical locations are illustrated in figure 3.9.

Table 3.1: Specifications of the eight cases, and disconnection events used in this thesis. The first four cases (1-4) are used to tune the frequency prediction model. The prediction model is then used to attempt to predict the frequency response of the last four cases (5-8).

Case	Location	Bus number	P_0[MW]	Q_0[MVAr]	M_{base}[MVA]
Case 1	Oskarshamn	3300	999	113	1000
Case 2	Ringhals	3359	1110	113	1000
Case 3	Kvildal	6000	736	113	1000
Case 4	Olkilouto	7000	1086	113	1000
Case 5	Oulu	7100	715	113	1000
Case 6	Forsmark	3000	1100	967	1300
Case 7	Oslo 2	5500	1132	81	1450
Case 8	Røssåga	6700	1753	99	2144

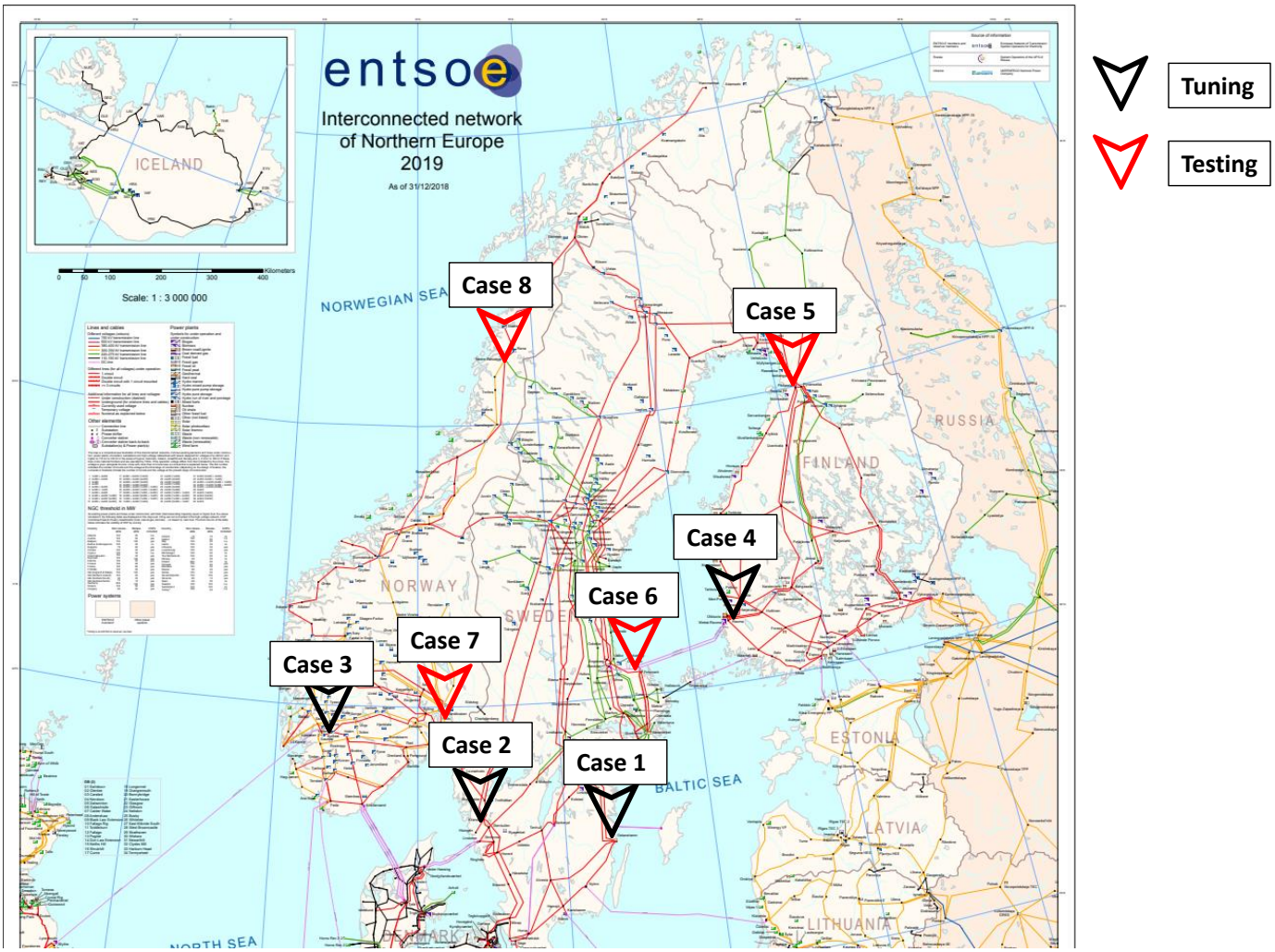

Figure 3.9: The location of the eight tune- and test cases used in the thesis. Tune cases, marked in black, have their response used to configure the prediction model. Test cases, marked in red, are attempted predicted and their response is used to evaluate precision [23].

The eight specific generators were identified in the PSSE N44 model and disconnected through the ePHASORSIM interface. For each case, the generator speed deviation of the remaining connected generators was recorded. The generators of the separate cases varied in location and size, which allowed for different system responses to be recorded. By configuring ePHASORSIM to output the speed deviation of all connected generators, the electrical frequency of the system could be recorded.

All cases, both test and tune cases eventually have each individual generator converge towards the same steady state value. This occurs when the system has been allowed to run for a substantial amount of time. Each machine converges to its owns steady state deviation based on the size of the power disturbance. After 400 seconds the system can be considered to being close to steady state, and so the value at $f(t) = 400\,\mathrm{s}$ is used to calculate this quantity.

The cases 1-4 are tune cases, and are used for tuning the two transfer functions $G_1(s)$ and $G_2(s)$. This is done by first taking the center of inertia frequency f_{coi} of the frequency response of each case. Then the free parameters of the transfer functions are tuned such that the step response coincides with the measured tune case response.

The four test cases are then used to test the completed transfer functions ability to predict frequency responses. A power disturbance P_d of the same size as the loss of generation P_0 in each case is chosen. This power disturbance P_d is calculated in per unit, with regards to the total rated power of the system $\sum_i^{N_G} M_{base,i}$. The disconnected machine for each case is excluded from this calculation.

Test cases were chosen for a range of different active delivered power. Case 5 is the smallest disturbance, cases 6 and 7 are average, and case 8 is the largest. They are also located at different electrical and geographical locations of the grid. Case 6 and 7 are located relatively central, whereas case 5 and case 8 are more on the outskirts of the electrical grid.

The frequency response of all cases are presented in chapter 4.

3.5 Center Of Inertia frequency $\mathbf{f_{coi}}$

The measured frequencies are aggregated into a single system response by use of the system frequency inertia f_{coi} (see section 2.3). This weighted average gives a representation of the general dynamics of the electrical frequency of the system. Each individual generator behaves independently, and oscillates around the f_{coi}. Oscillations are largest right after the disturbance. As time passes the oscillations die out and the individual signals converge towards the f_{coi}.

Case 1 is used to illustrate how f_{coi} follows the individual machine responses. A comparison of the individual machine frequencies to the system frequency approximation f_{coi} is shown in figure 3.10 for the first 20 seconds following the disturbance. The disconnected generator is removed from the active set $\mathcal{A}$ and is not included when calculating f_{coi}. In the plot the disconnected generator can be recognized as the machine with a constant frequency $f = 50\,\text{Hz}$. This is due to its measured speed deviation being zero, due to it being disconnected, and so no frequency deviation is calculated.

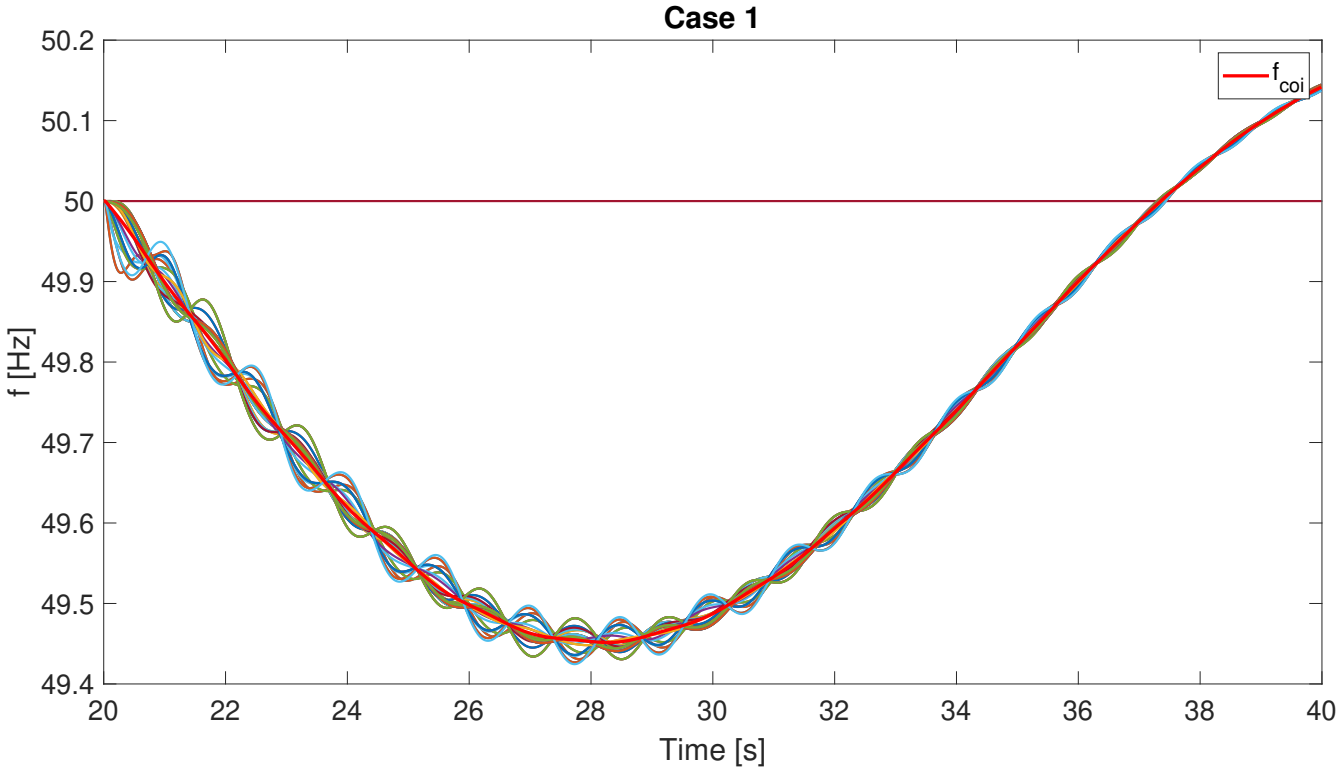

Figure 3.10: The center of inertia frequency shown in thick red along with the individual machine responses, for the first system swing of case 1. The center of inertia frequency f_{coi} is a weighted average of the individual machine frequencies, where the weights are based on the kinetic energy of each machine.

3.6 Primary response modelling

In the following section a method for estimating the frequency nadir following a power disturbance is presented.

The frequency nadir Δf_{max} can be estimated through modelling of a system wide transfer function $G(s) = \frac{\Delta f}{P_d}(s)$. Here, a power disturbance P_d can be considered as the input of the transfer function block, giving the output Δf. Two methods for developing system transfer functions are presented in section 2.8. The first model represents a Proportional-controller (P-controller). The second model adds integral effect for a proportional-integral-controller (PI-controller). The two governor transfer functions G_{gov} are are referred to respectively as G_P and G_{PI}, and are repeated below:

$$G_P = -K\frac{1}{Ts+1} \tag{3.3a}$$

$$G_{PI} = -K\frac{1+T_1 s}{(1+T_2 s)(1+T_3 s)} \tag{3.3b}$$

Combining the governor models in (3.3) with the swing equation in (**??**) gives two possible expressions for systems dynamics. Mathematical manipulation allows for the two system transfer functions $G_1(s)$ and $G_2(s)$, respectively based on the P and PI governor models. $G_1(s)$ is a second order transfer function, while $G_2(s)$ is a third order transfer function. The two system transfer functions are repeated below:

$$G_1(s) = \frac{\frac{1}{2H}s + \frac{1}{2HT}}{s^2 + \frac{1}{T}s + \frac{K}{2HT}} \tag{3.4a}$$

$$G_2(s) = \frac{\frac{1}{2H}s^2 + \frac{T_2+T_3}{2HT_2T_3}s + \frac{1}{2HT_2T_3}}{s^3 + \frac{T_2+T_3}{T_2T_3}s^2 + \frac{(2H+KT_1)}{2HT_2T_3}s + \frac{K}{(2H+KT_1)}} \tag{3.4b}$$

3.6.1 Choice of inertia for tuning

Calculation of system inertia H_{sys} from PSSE values leads to a predicted initial slope that is less steep than what can be seen from the f_{coi} simulations. Instead of using the calculated inertia value in the transfer function tuning, a new freely chosen inertia H_{free} was used. As shown in figure 3.11 this gives a better fit with the initial slope in all cases. The freely chosen inertia values is summarized in the table below:

Table 3.2: System inertia values H_{sys} from PSSE machine values, and freely chosen system inertia values H_{free} chosen from best fit. The free values are used for the tuning of transfer functions $G_1(s)$ and $G_2(s)$.

	Case 1	Case 2	Case 3	Case 4
H_{sys} [s]	4.27	4.29	4.31	4.27
H_{free} [s]	3.7	3.7	4	4.2

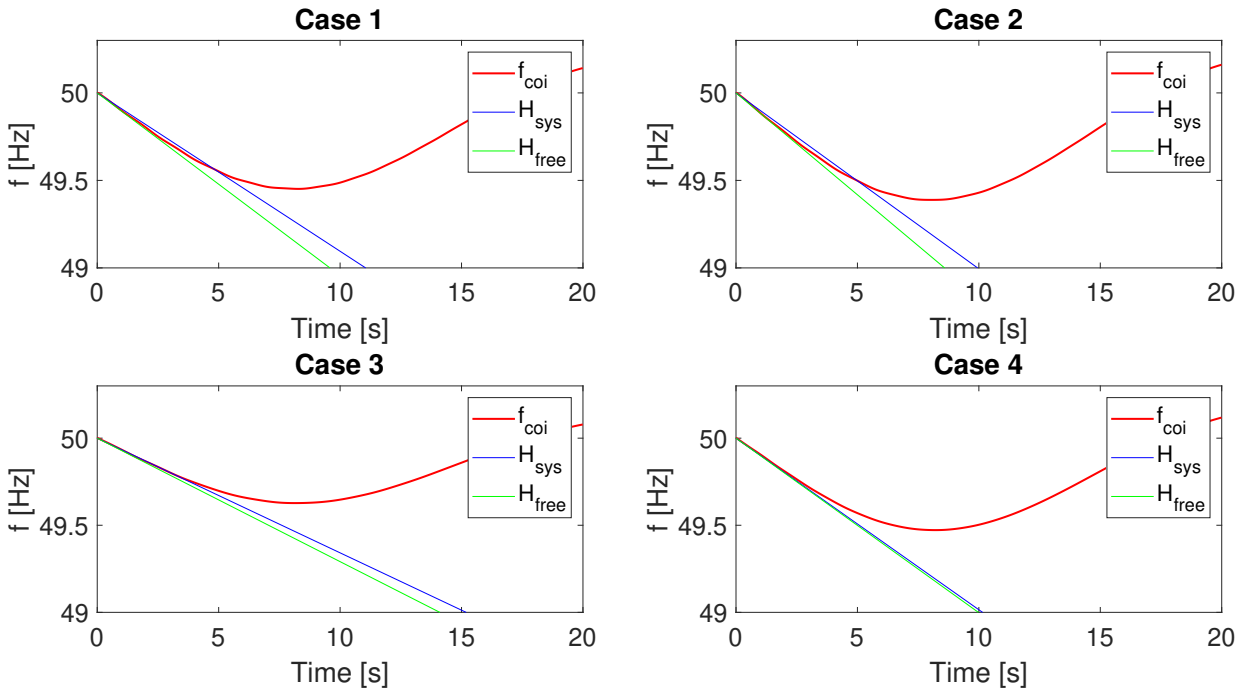

Figure 3.11: Calculated system inertia is used with the swing equation to estimate the steepness of frequency development following a fault. The freely chosen inertia used in tuning H_{free} is shown as along with H_{sys}, which is found from the PSSE model, and the simulated system frequency f_{coi}.

Chapter 4

Results

4.1 Cases

The full 400 second simulation is shown for cases 1-4 in figure 4.1, and for cases 5-8 in figure 4.2. The first system swing following the disturbance is shown from 20-40 seconds for case 1-4 in figure 4.3 and for case 5-8 in figure 4.4. The aggregated system frequencies are shown afterwards in the form of the calculated center of inertia frequency f_{coi}. Only the first swing is shown, for cases 1-4 in figure and cases 5-8 in figure. The system swing time for every case is roughly 28-29 seconds for all cases.

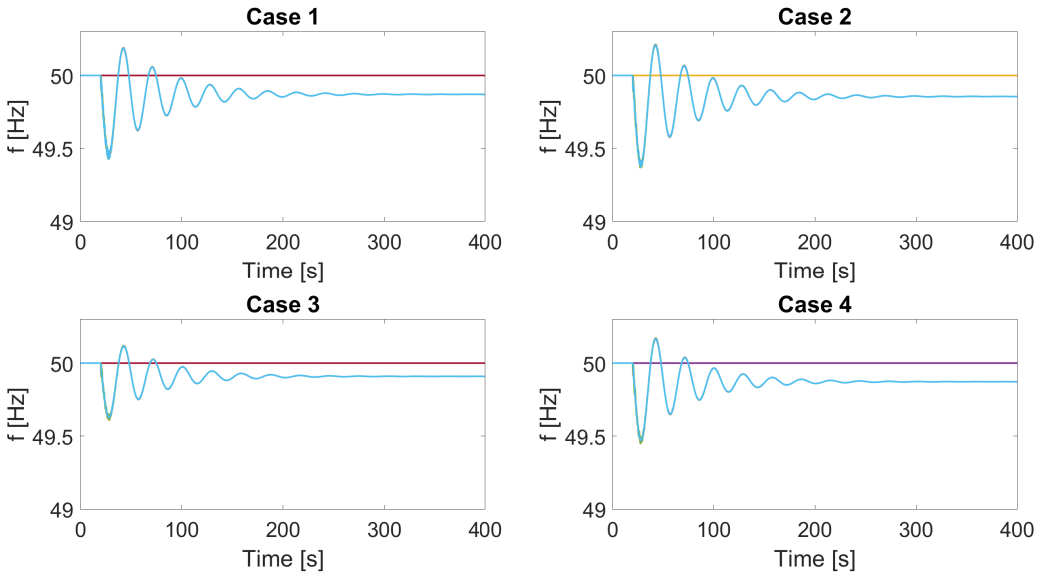

Figure 4.1: The electrical frequency of all generators following each of the four tune cases (1-4). The full 400 seconds of simulation is shown. Individual machines can be seen to oscillate against each other and eventually converge as more time passes.

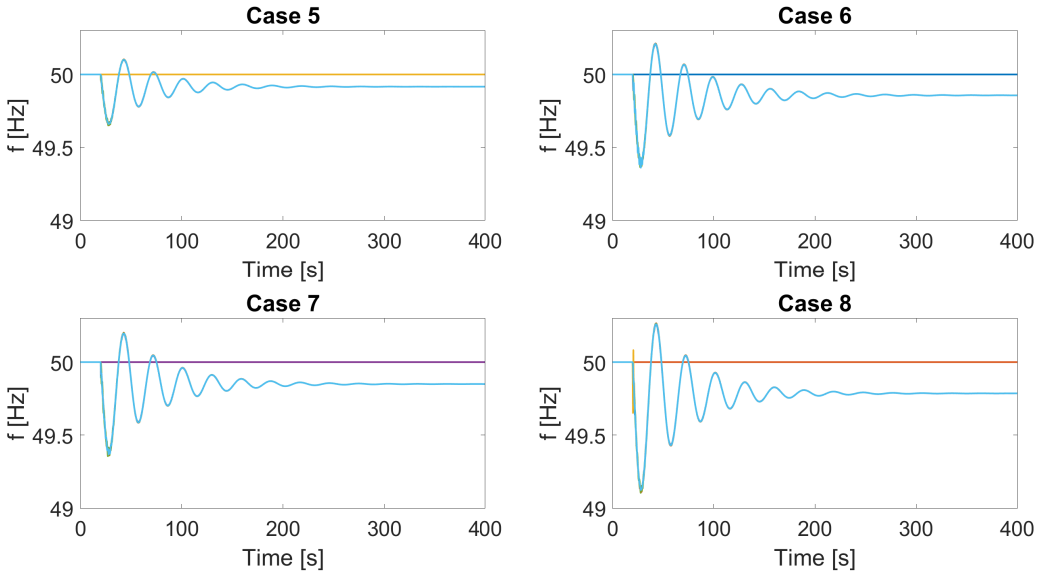

Figure 4.2: The electrical frequency of all generators following each of the four test cases (5-8). The full 400 seconds of simulation is shown. Individual machines can be seen to oscillate against each other and eventually converge as more time passes.

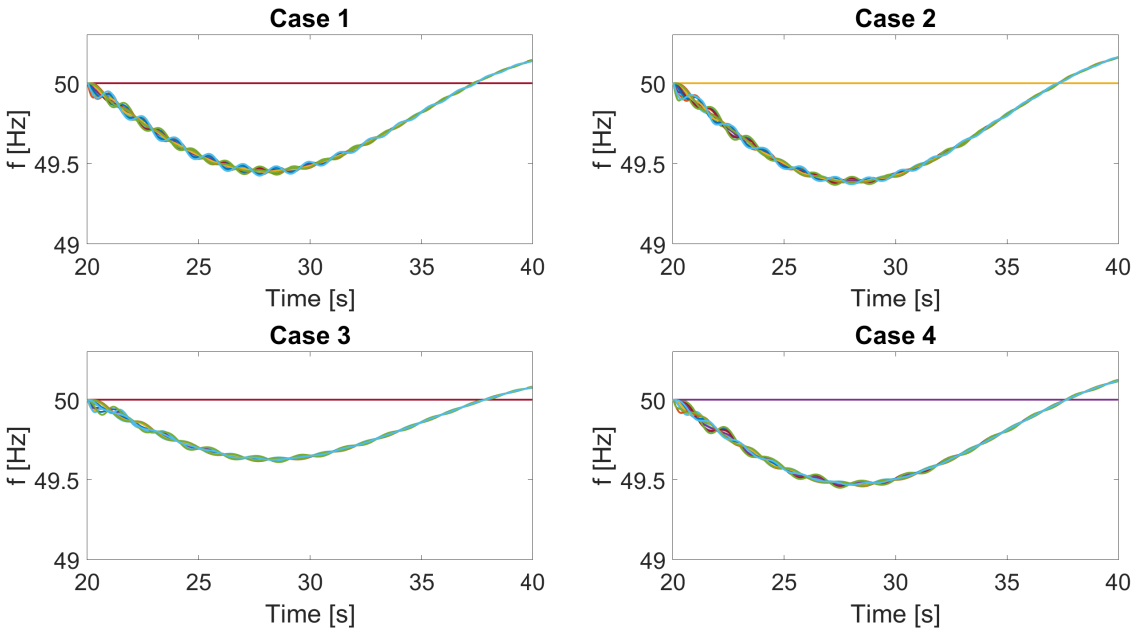

Figure 4.3: The electrical frequency of all generators following each of the four tune cases (1-4). Only the first system swing is shown. Individual machines can be seen to oscillate against each other and eventually converge as more time passes.

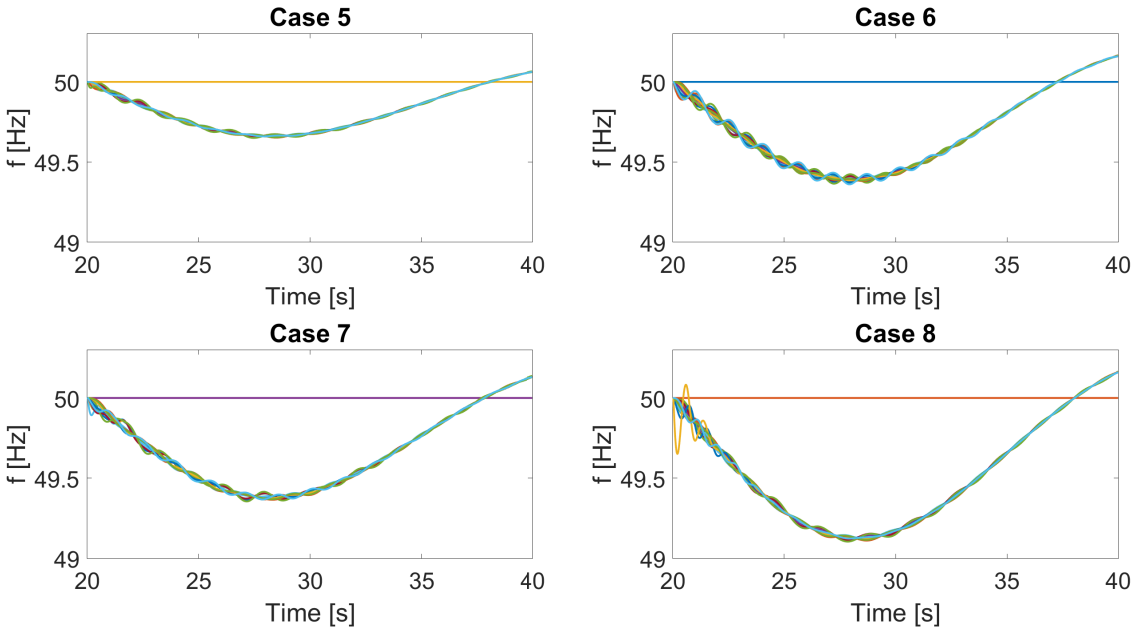

Figure 4.4: The electrical frequency of all generators following each of the four test cases (5-8). Only the first system swing is shown. Individual machines can be seen to oscillate against each other and eventually converge as more time passes.

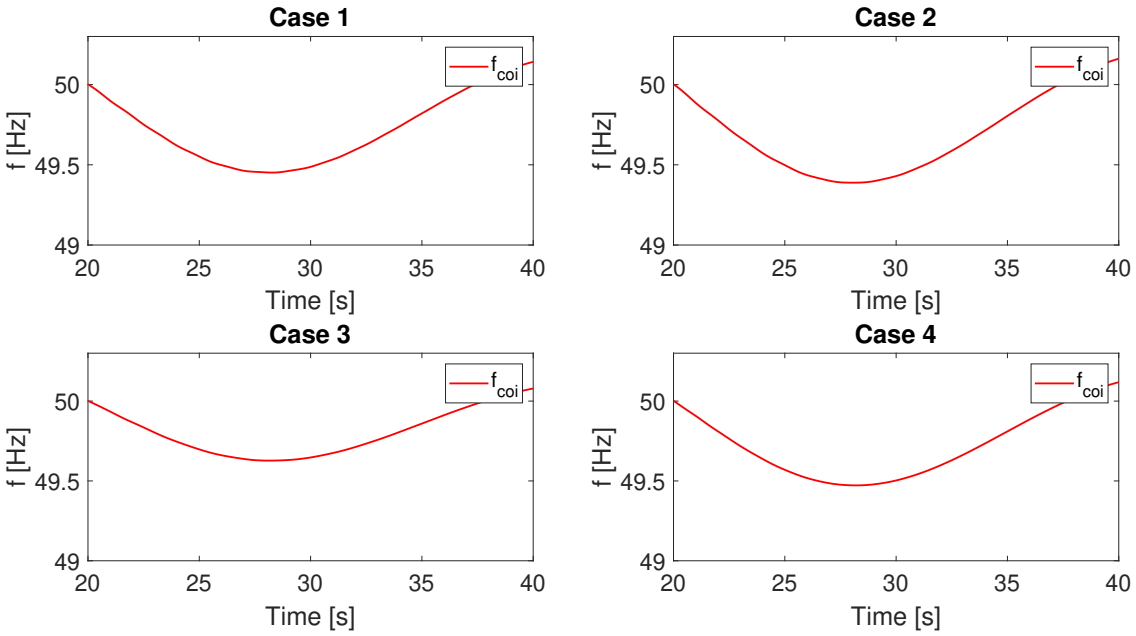

Figure 4.5: The center of inertia frequency f_{coi} following each of the four tune cases (1-4). Only the first system swing is shown.

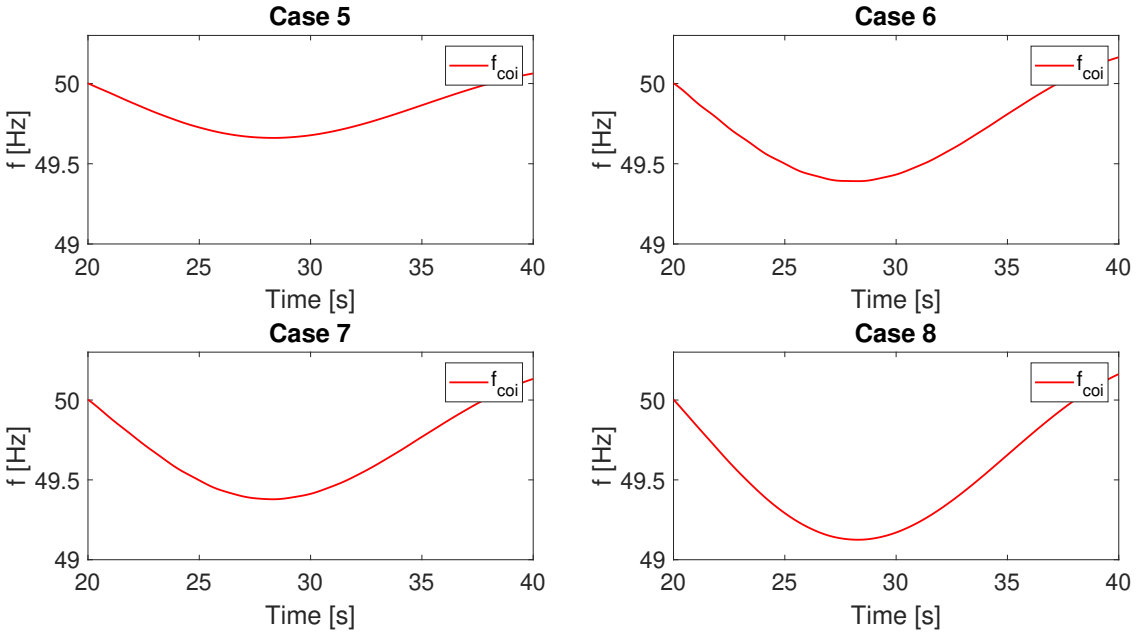

Figure 4.6: The center of inertia frequency f_{coi} following each of the four test cases (5-8). Only the first system swing is shown.

4.1.1 System inertia H_{sys}

The system inertia H_{sys} can be calculated for each case from the machine values in the PSSE N44 model. This is done by disregarding the disconnected governor, and calculating inertia from the connected rated energy divided by the connected rated power. Equation (2.7) in section 2.2 can be used. The inertia prior to any disturbances can also be calculated by not excluding any of the machines in the calculation. As can be seen from 4.1, the system inertia H_{sys} is around 4.3 s for all cases.

Table 4.1: System inertia H_{sys} calculated from the PSSE values of the model.

Case	H_{sys}
Base case	4.296
Case 1	4.267
Case 2	4.285
Case 3	4.307
Case 4	4.272
Case 5	4.313
Case 6	4.262
Case 7	4.325
Case 8	4.320

4.1.2 Active power disturbance P_d

Using the total rated power of all connected generators S_{sys} as a base, we can calculate the per unit power disturbance for all cases. The active power disturbance for each case is presented in the table below. We consider a generator disconnection like a step response, going from delivering active power P_0 to delivering zero active power the next instant. The system experiences this loss of generation event as a net negative generated power.

Table 4.2: Active power disturbance P_d for all cases given in absolute value. The system sees the disturbance as a net negative power disturbance. Per unit value is calculated from the sum of rated power of connected machines post fault.

Case	$\|P_d\|$ [MW]	$\|P_d\|$ [per unit]	S_{tot} [GW]
Case 1	999	15.45e-3	64.66
Case 2	1110	17.23e-3	64.41
Case 3	736	11.35e-3	64.87
Case 4	1086	16.84e-3	64.49
Case 5	715	11.04e-3	64.76
Case 6	1100	17.06e-3	64.46
Case 7	1132	17.60e-3	64.31
Case 8	1753	27.55e-3	63.62

4.1.3 Maximum frequency deviations and steady state deviations

The general size of the disturbances could be quantified through the maximum frequency deviation, Δf_{max}, and the steady state frequency deviation Δf_{∞}. In order to approximate these metrics, the system frequency was aggregated into its center of inertia frequency f_{coi}. Its first nadir was used to record the maximum deviation, and steady state frequency deviation was recorded at 400 seconds of simulation time. The center of inertia frequency and the two metrics are illustrated for case 8 in figure 4.7. The maximum frequency deviation and steady state frequency deviations of all cases are summarized in 4.3 below.

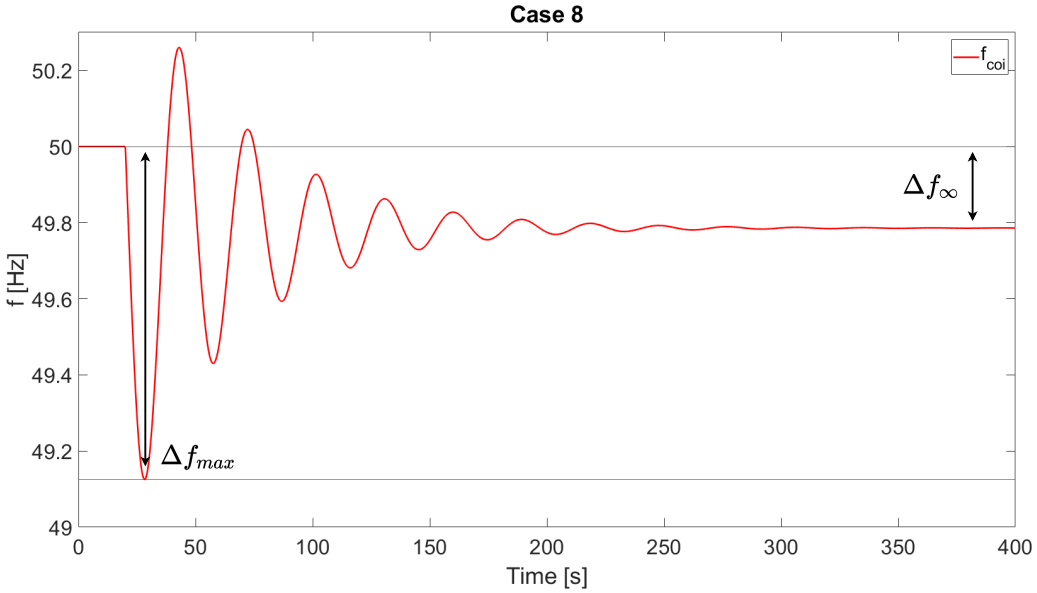

Figure 4.7: Illustration of maximum frequency deviation and steady state deviation

Table 4.3: Summary Δf_{coi} all cases.

Case	$\Delta f_{max}[Hz]$	$\Delta f_{\infty}[Hz]$
Case 1	0.55	0.13
Case 2	0.61	0.14
Case 3	0.37	0.09
Case 4	0.53	0.17
Case 5	0.34	0.08
Case 6	0.61	0.14
Case 7	0.62	0.15
Case 8	0.87	0.23

4.2 Tuning

4.2.1 Tuning $G_1(s)$

Tuning of system transfer function $G_1(s)$ from (3.4a) was performed. $G_1(s)$ is repeated below for the convenience of the reader.

$$G_1(s) = \frac{\frac{1}{2H}s + \frac{1}{2HT}}{s^2 + \frac{1}{T}s + \frac{K}{2HT}}$$

Tuning was performed with system inertia H chosen as a free variable. The chosen values was found through visual comparison and repeated minor adjustments to the variable. When the initial slope of the step response of was close to parallel with the initial slope of the system frequency f_{coi}. The same values were used for $G_2(s)$, when inertia H was found from visual inspection. K was based on the estimated system frequency bias, calculated from $P_d/\Delta f_\infty$. The T variable was repeatedly adjusted until the maximum frequency deviations of step response and f_{coi} coincided. The two figures, 4.8 and 4.9 show the 20 seconds and 380 second comparison between step response and simulated system frequency f_{coi}. The tuned variables are presented in table 4.6.

Table 4.4: Tuning step response for g2(s)

	H	K	T
Case 1	3.7	5.94	19.8
Case 2	3.7	5.95	19.8
Case 3	4	6.25	19.2
Case 4	4.2	6.60	19.4

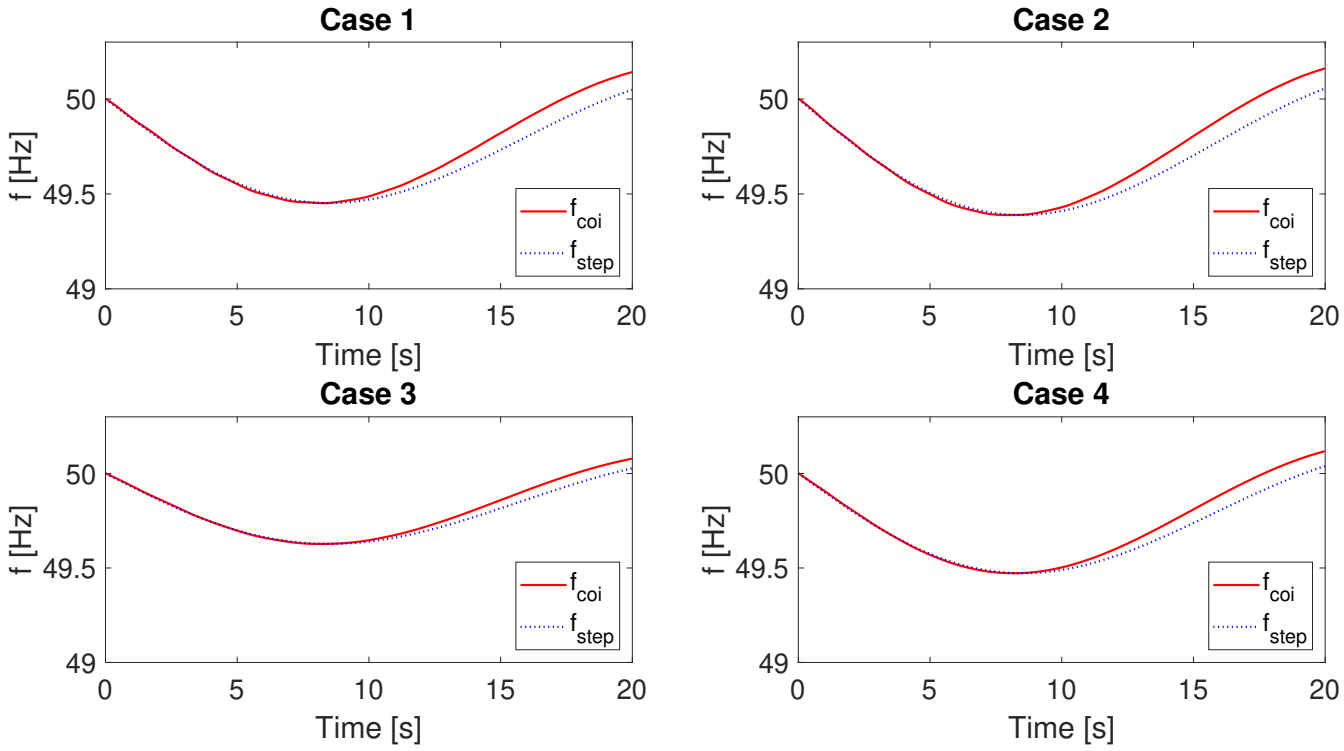

Figure 4.8: Tuning of the step response f_{step} from $G_1(s)$ with inertia chosen from the best visual fit, for the first 20 seconds following the disturbance for all 4 tuning cases.

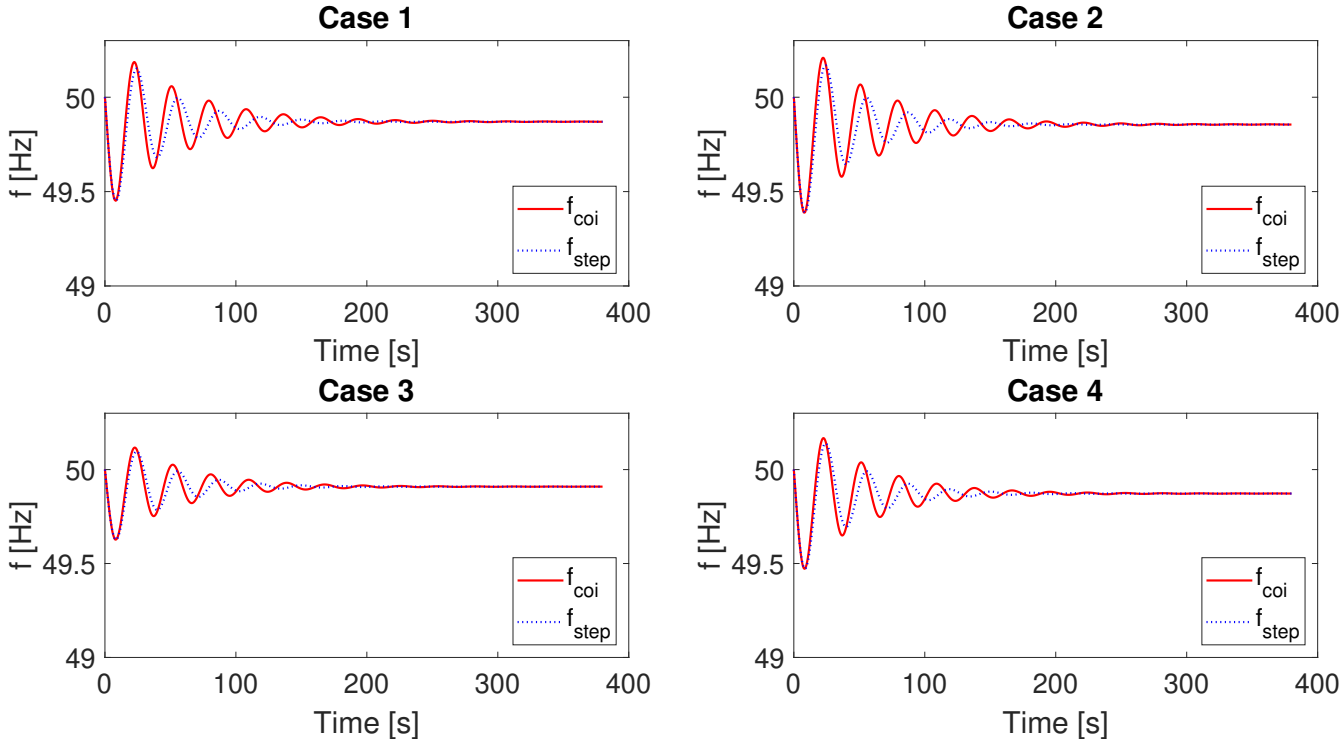

Figure 4.9: Tuning of the step response f_{step} from $G_1(s)$ with inertia chosen from the best visual fit, for the full 380 seconds following the disturbance for all 4 tuning cases.

4.2.2 Tuning $G_2(s)$

Tuning of system transfer function $G_2(s)$ from (3.4b) was performed. $G_2(s)$ is repeated below for the convenience of the reader.

$$G_2(s) = \frac{\frac{1}{2H}s^2 + \frac{T_2+T_3}{2HT_2T_3}s + \frac{1}{2HT_2T_3}}{s^3 + \frac{T_2+T_3}{T_2T_3}s^2 + \frac{(2H+KT_1)}{2HT_2T_3}s + \frac{K}{(2H+KT_1)}}$$

Tuning was performed with system inertia H chosen as a free variable. The chosen values was found through visual comparison and repeated minor adjustments to the variable. When the initial slope of the step response of was close to parallel with the initial slope of the system frequency f_{coi}. The same values were used for $G_2(s)$, when inertia H was found from visual inspection. K was based on the estimated system frequency bias, calculated from $P_d/\Delta f_\infty$. The T_1 and T_2 variables were repeatedly adjusted until the maximum frequency deviations of step response and f_{coi} coincided. The first half of the system swing was also attempted to be accurately represented, and prioritized over accuracy after the nadir. T_3 was set to 1 for all simulation. This was assumed a typical value for T_g servomotor time constant, which it represents. The two figures, 4.10 and 4.11 show the 20 seconds and 380 second comparison between step response and simulated system frequency f_{coi}. The tuned variables are presented in table 4.7.

Table 4.5: Tuning step response for g2(s)

	H	K	T_1	T_2	T_3
Case 1	3.7	5.94	0.35	16.1	1
Case 2	3.7	5.95	0.3	16	1
Case 3	4	6.25	0.45	16.2	1
Case 4	4.2	6.60	0.4	16.1	1

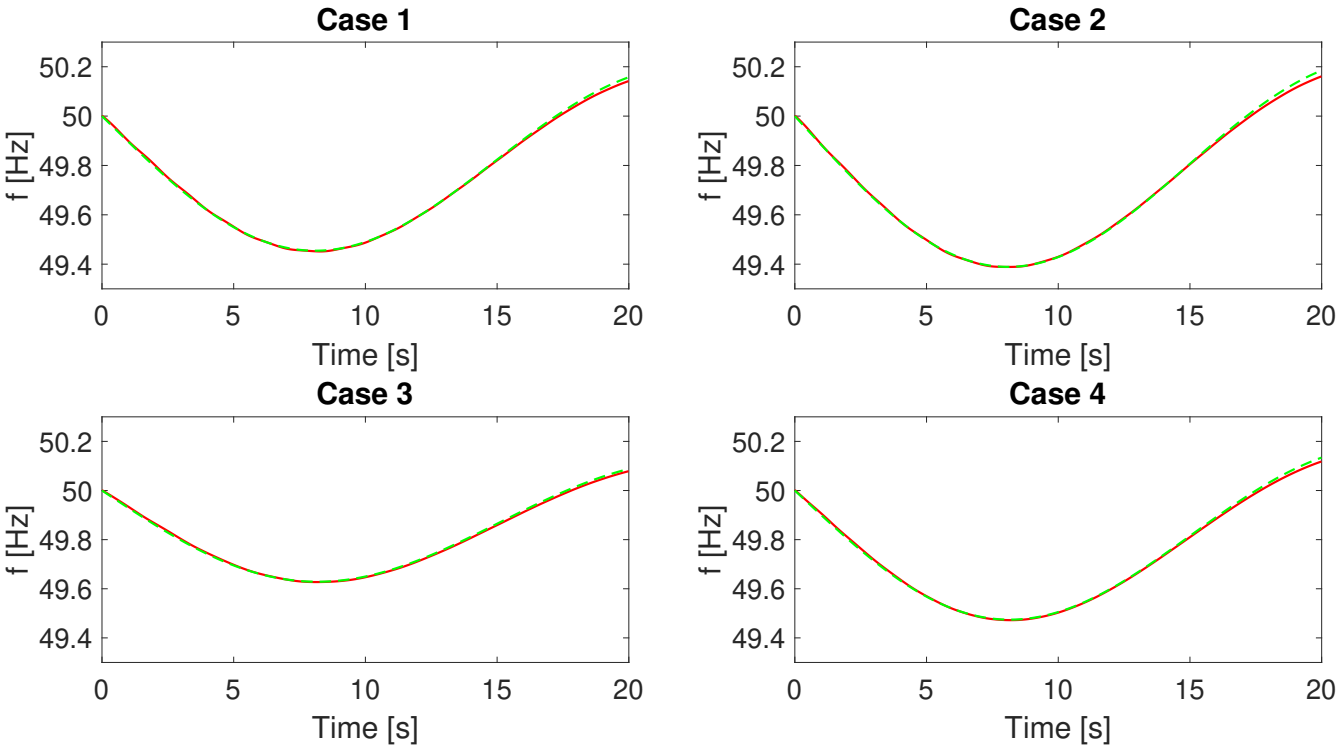

Figure 4.10: Tuning of the step response f_{step} from $G_2(s)$ with inertia chosen from the best visual fit, for the first 20 seconds following the disturbance for all 4 tuning cases.

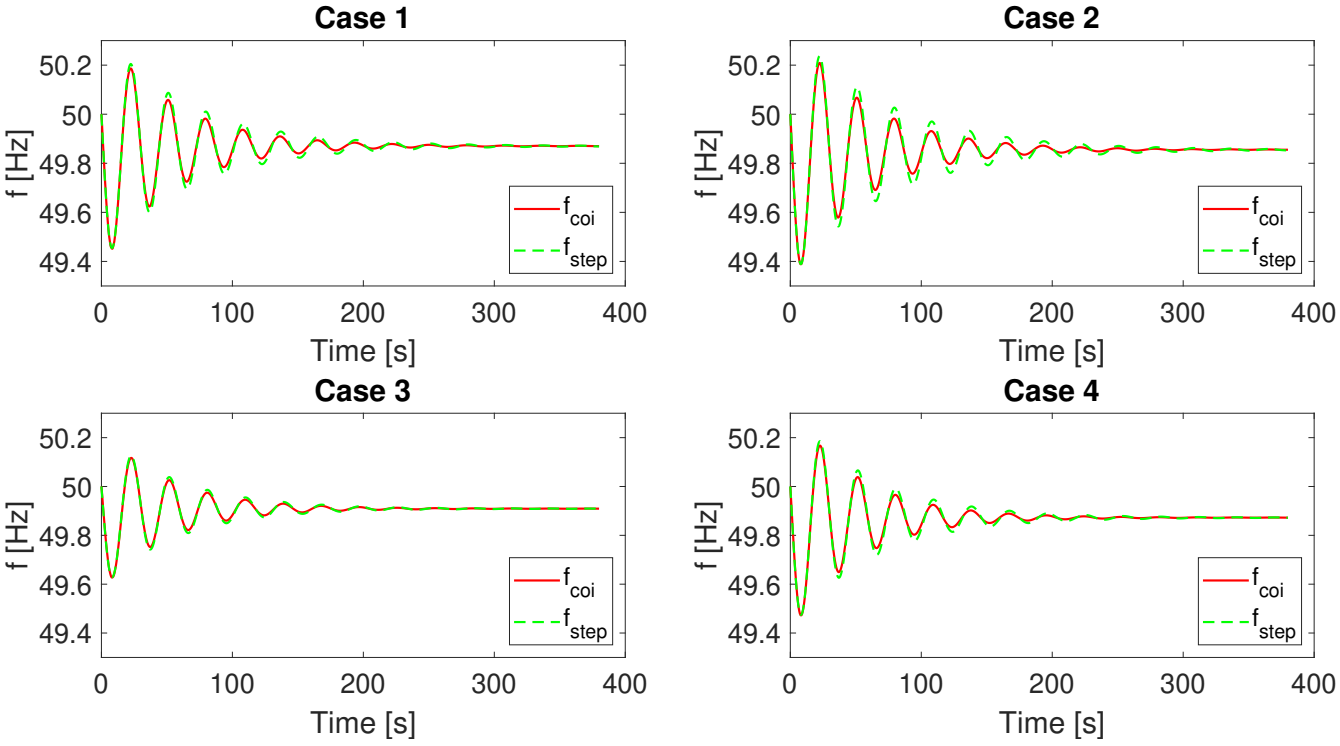

Figure 4.11: Tuning of the step response f_{step} from $G_2(s)$ with inertia chosen from the best visual fit, for the full 380 seconds following the disturbance for all 4 tuning cases.

4.2.3 Predictions

The tuned transfer functions can now be used to predict the frequency response of the test cases (5-8). Each of the two transfer functions $G_1(s)$ and $G_2(s)$ have 4 different tuned version, based on the tune cases (1-4). The tuning of the transfer function will be referred to by a second subscript. As an example, G_{23} refers to $G_2(s)$ tuned from case 3, and G_{14} refers to $G_1(s)$ tuned from case 4.

Table 4.6: Tuned parameters for $G_1(s)$

	H	K	T
Case 1	3.7	5.94	19.8
Case 2	3.7	5.95	19.8
Case 3	4	6.25	19.2
Case 4	4.2	6.60	19.4

Table 4.7: Tuned parameters for G2

	H	K	T_1	T_2	T_3
Case 1	3.7	5.94	0.2	15.5	1
Case 2	3.7	5.95	0.2	15.5	1
Case 3	4	6.25	0.5	16.5	1
Case 4	4.2	6.60	0.4	16.3	1

Predictions from Case 1 tuning

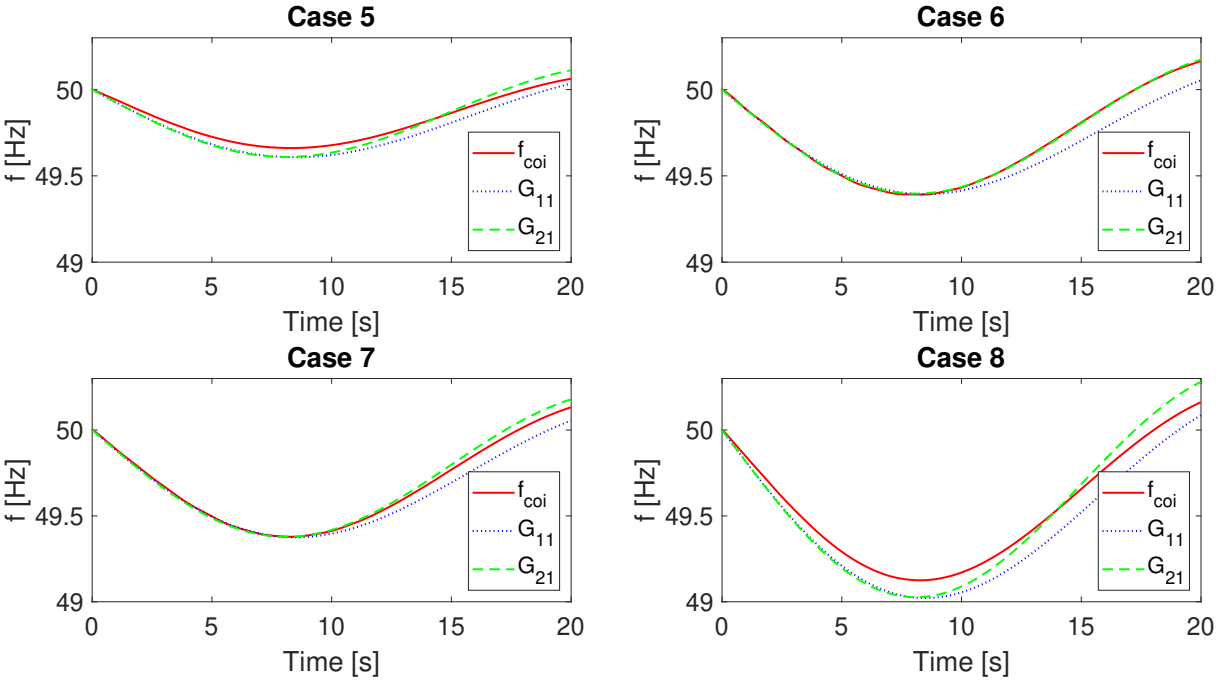

Figure 4.12: Prediction of test cases based on case 1 tuning of transfer function G1 and G2

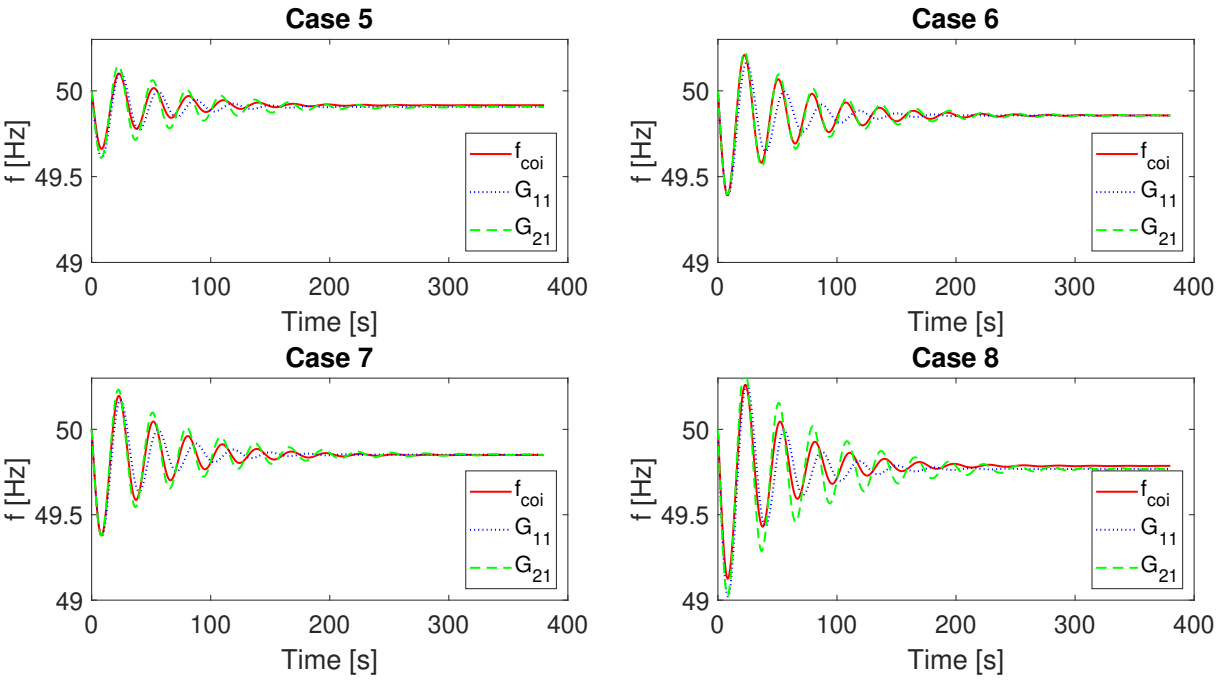

Figure 4.13: Prediction of test cases based on case 1 tuning of transfer function G1 and G2

Predictions from Case 2 tuning

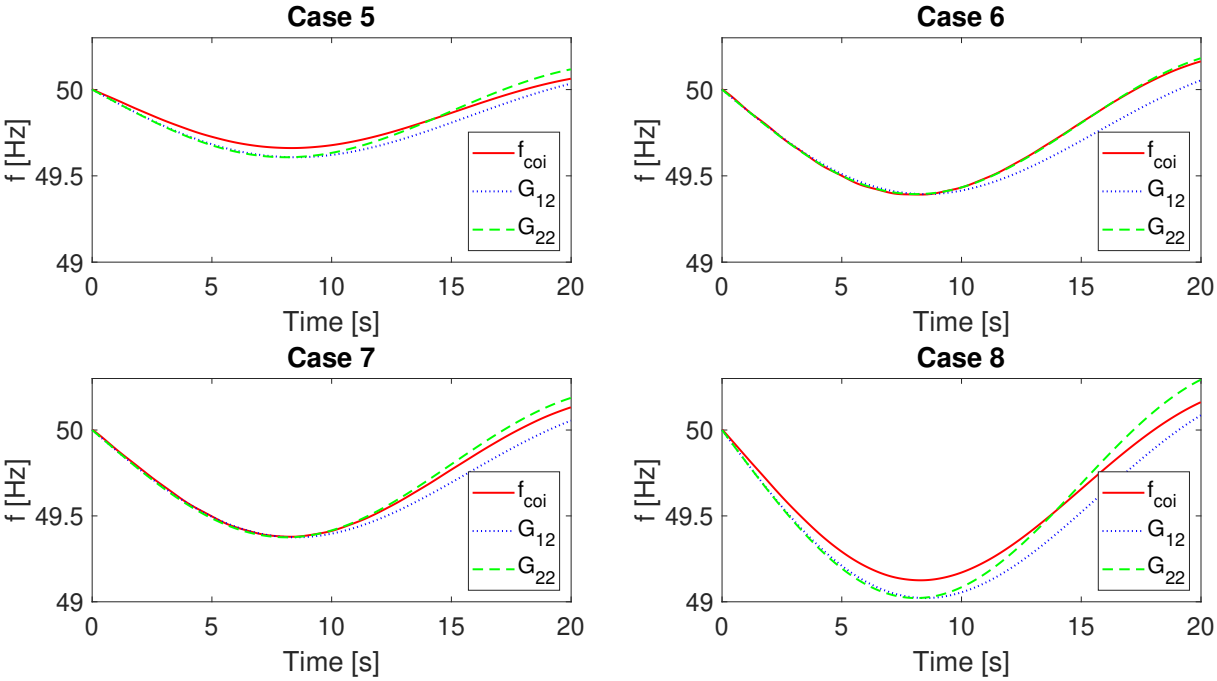

Figure 4.14: Prediction of test cases based on case 2 tuning of transfer function G1 and G2

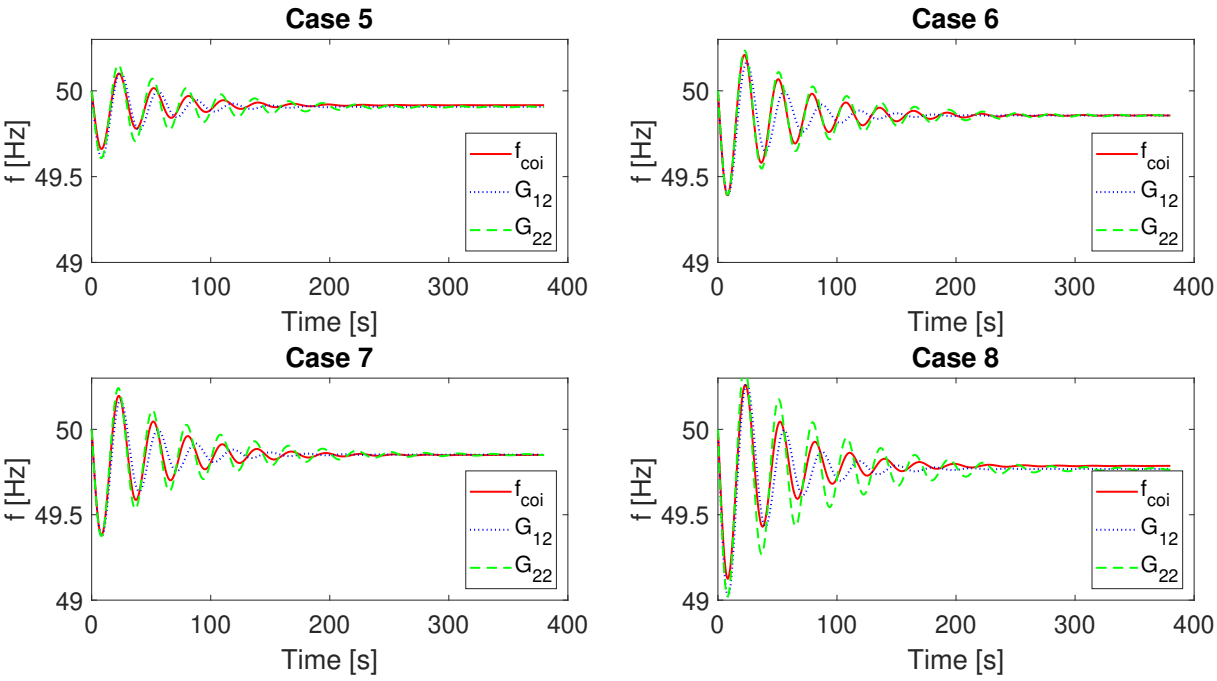

Figure 4.15: Prediction of test cases based on case 2 tuning of transfer function G1 and G2

Predictions from Case 3 tuning

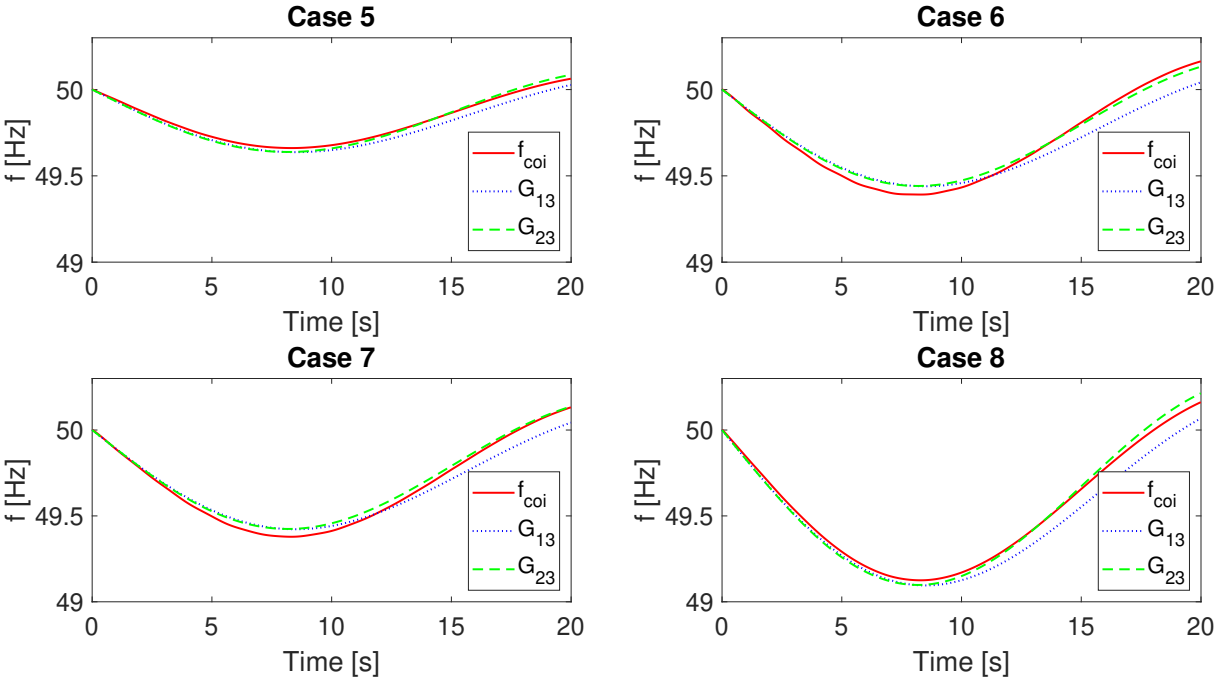

Figure 4.16: Prediction of test cases based on case 3 tuning of transfer function G1 and G2

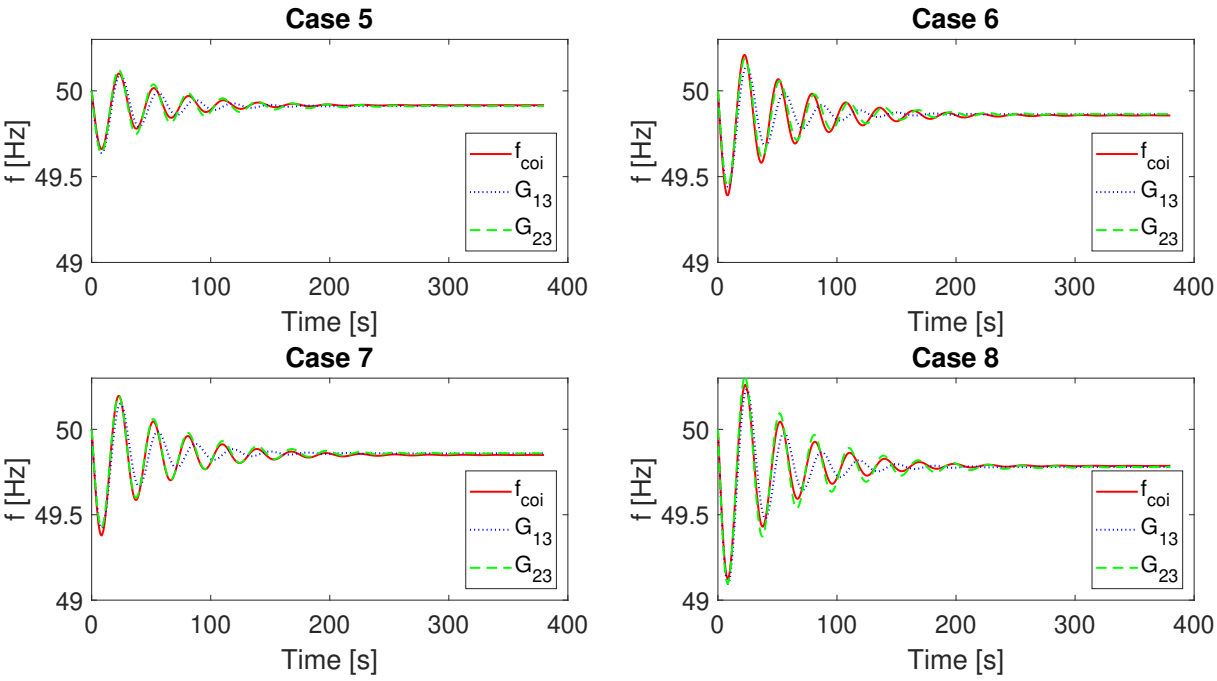

Figure 4.17: Prediction of test cases based on case 3 tuning of transfer function G1 and G2

Predictions from Case 4 tuning

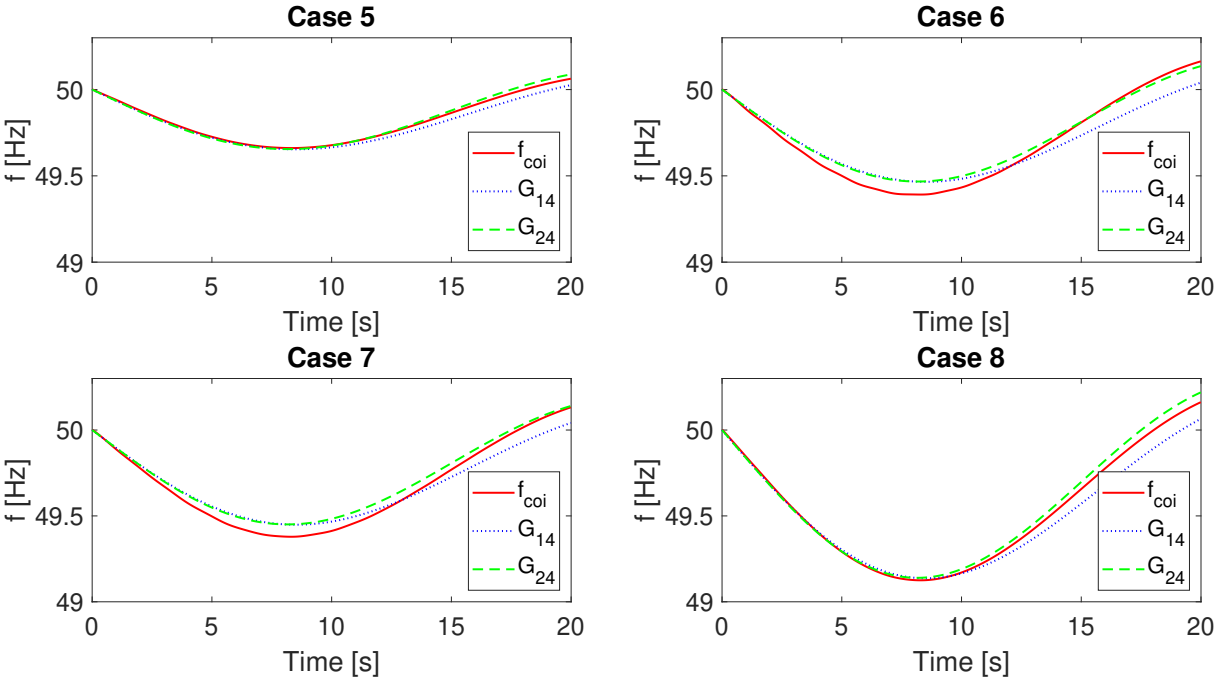

Figure 4.18: Prediction of test cases based on case 4 tuning of transfer function G1 and G2

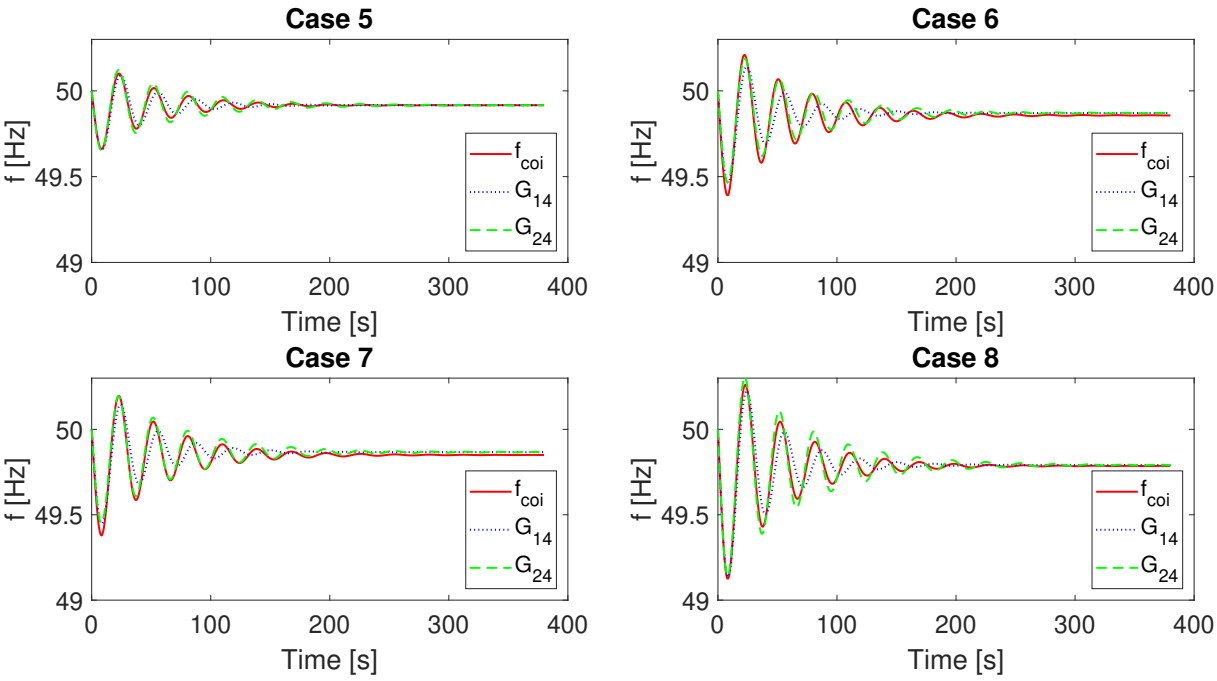

Figure 4.19: Prediction of test cases based on case 4 tuning of transfer function G1 and G2

4.3 Prediction accuracy

4.3.1 Prediction error - value

The deviation e_{nadir} between the predicted nadir and nadir of the corresponding f_{coi} is shown in the table below. The mean absolute error of the nadir estimation is 39.5 mHz with a standard deviation of 34.2 mHz.

Table 4.8: Deviation between predicted and measured nadir e_{nadir} [mHz].

Transfer function	Case 5	Case 6	Case 7	Case 8
G_{11}	-53	3	-3	-103
G_{21}	-51	5	0	-99
G_{12}	-53	3	-3	-103
G_{22}	-53	3	-3	-103
G_{13}	-24	48	44	-30
G_{23}	-23	50	45	-27
G_{14}	-7	70	70	12
G_{24}	-6	72	72	14

Table 4.9: Average absolute error between predicted and measured nadir e_{max} [mHz].

Transfer function	Average deviation
G_{11}	41
G_{21}	39
G_{12}	41
G_{22}	41
G_{13}	36
G_{23}	36
G_{14}	41
G_{24}	42

4.3.2 Prediction error - time deviation

The time deviation Δt_{nadir} between the occurrence of the predicted nadir and the nadir of the corresponding f_{coi} is shown in the table below.

Table 4.10: Time deviation between predicted and measured nadir Δt_{min} [s]

Transfer function	Case 5	Case 6	Case 7	Case 8
G_{11}	0.16	0.21	0.19	0.21
G_{21}	-0.24	-0.19	-0.21	-0.19
G_{12}	0.16	0.21	0.19	0.21
G_{22}	-0.23	-0.18	-0.20	-0.18
G_{13}	0.17	0.22	0.20	0.22
G_{23}	-0.16	-0.11	-0.13	-0.11
G_{14}	0.18	0.23	0.21	0.23
G_{24}	-0.17	-0.12	-0.14	-0.12

Table 4.11: Average absolute time deviation between predicted and measured nadir Δt_{min} [s]

Transfer function	Average time deviation
G_{11}	0.19
G_{21}	0.21
G_{12}	0.19
G_{22}	0.20
G_{13}	0.20
G_{23}	0.13
G_{14}	0.21
G_{24}	0.14

Chapter 5

Discussion and conclusion

5.1 Individual generator swings

The availability of the system frequency, expressed as center of inertia frequency f_{coi}, is not given. Local frequencies oscillate around the system frequency due to the turbine rotor oscillations. To exemplify this we look at the frequency response of the individual machines from case 8. This disconnection represents a disconnection of a generator initially delivering 1753 MW. This is much larger than both hydro power plants in Røssåga, that combine for 520 MW [24][25], and is a hypothetical test case for the system. This is also larger than the dimensioning incident indicated by entso-e at 1450 MW for the Nordic synchronous area [26].

The system frequency is plotted next to machine response of the 38th connected generator in figure 5.1. This corresponds to generator at bus 6700 which is the second connected generator at Røssåga, besides the one that is being disconnected in case 8. This is both the closest generator, electrically, and the generator is represented as abnormally large. This means that a lot of power is drawn from the machine once the disconnection occurs. The machine continues oscillating around the signal for 4 large swings before converging around the system frequency after 2-4 seconds. Due to damping of the oscillations when the system frequency reaches it's minimum, the local differences in electrical frequency can mostly be neglected.

To calculate the exact system frequency, one would need measurements from a sufficient amount of generators throughout the system. This may not be possible, as accurate measurement units may not have have been implemented. However, quite accurate methods for system frequency estimation exist, for example based on the inflection points of the oscillations of a single frequency measurement [27].

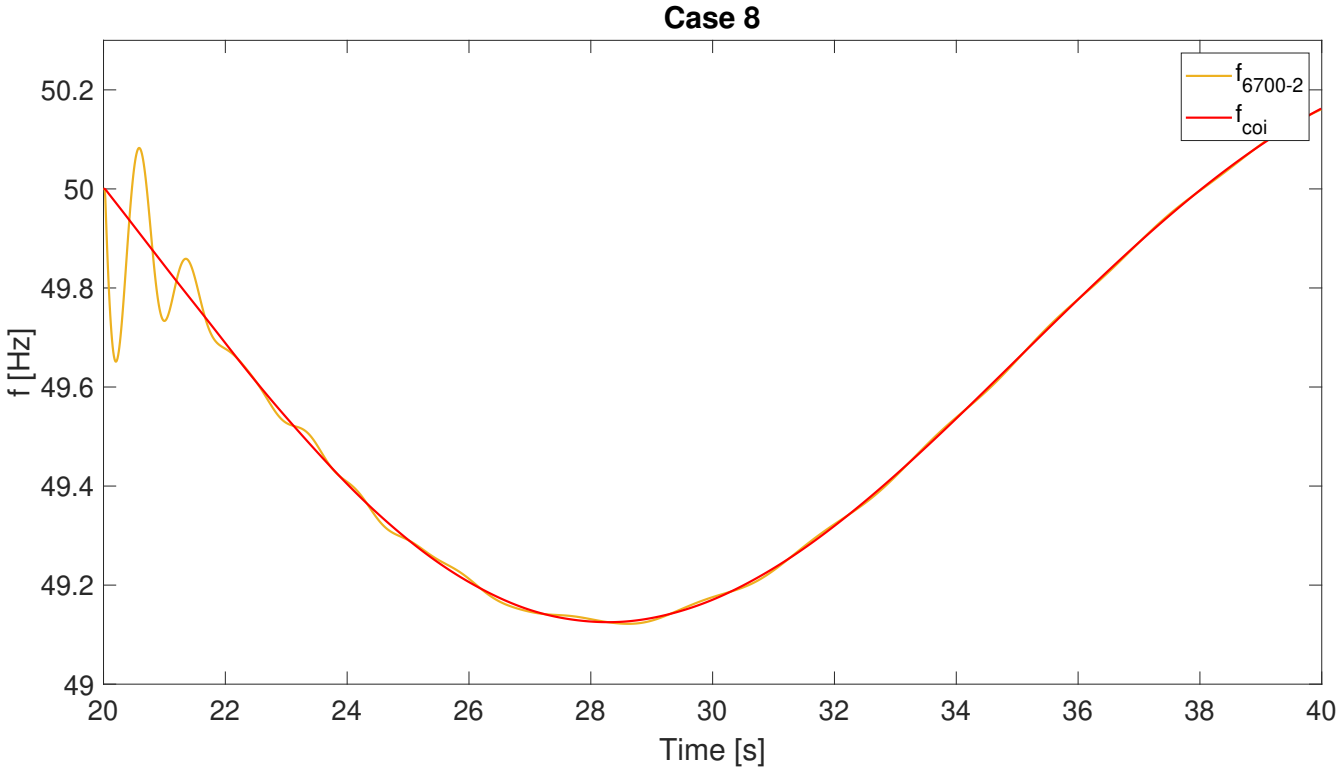

Figure 5.1: Case 8 individual dynamics of machine 38 vs system response

5.2 Tuning

5.2.1 Tuning $G_1(s)$

With the proposed method the transfer function $G_1(s)$ could accurately be fitted to correspond well with the frequency drop of all cases used for tuning (1-4).

The slope could be approximated by choosing the inertia constant H with the best possible fit. Initial attempts were attempted using H_{sys} calculated, but as shown in section 3.6.1 this gave poor results for fitting the first system swing. It is assumed that the reason for the discrepancy between measured and estimated intial RoCoF from H_{sys} is due to the simplifications made when aggregating the system into a single machine. The discrepancy was quite large for cases 1 and 2 which, had H_{sys} been used for tuning, would have lead to large deviations in initial slope. For prediction methods of the type presented in this thesis to work, sufficiently accurate inertia estimation tools are therefore crucial. Further work could look into how to best predict and accurately represent the system inertia and RoCoF following disturbances.

The K constant was tuned based on the method using the system gain presented in section 2.9. This tuning can be seen as odd for the $G_1(s)$ transfer function, due to the model representation being of a simple gain block in series with a servo-motor, and thus no droop feedback loop being present within the governor model itself. This tuning nevertheless captured the steady state dynamics of the system which was seen as beneficial. The results of tuning H and K like this meant that there was only one variable left.

The time constant T was tuned last, and used to fit the first swing of the prediction model to the frequency drop. Since T was the only remaining free variable, the first swing of the transfer function could not be fitted to accurately follow the measured response after the nadir. The time deviation of the frequency drop was also slightly off, compared to that of $G_2(s)$ tuning, but so small that it was considered insignificant. Trying fit secondary priorities with only the T variable was not possible without missing the main goal of predicting the frequency drop. The first half of the swing, which is the most crucial phase of the disturbance could still be accurately represented for all cases, and the tuning was considered satisfactory.

5.2.2 Tuning $G_2(s)$

With the proposed tuning method the transfer function $G_2(s)$ was able accurately capture the frequency drop in a similar fashion as $G_1(s)$. However, in addition it was also possible to accurately capture the ensuing system oscillations. System inertia was first estimated in the same way as for $G_1(s)$, through visual inspection of the RoCoF immediately following the fault. Then, keeping T_3 constant, the system oscillations could be lined up by adjusting the T_2 parameter. Finally, the T_1 parameter could be used to adjust the transfer function had an accurate representation of the first swing, capturing the frequency drop. The tuning of case 3 for the full 400 seconds of simulation (380 seconds following the disturbance) is shown in figure 5.2.

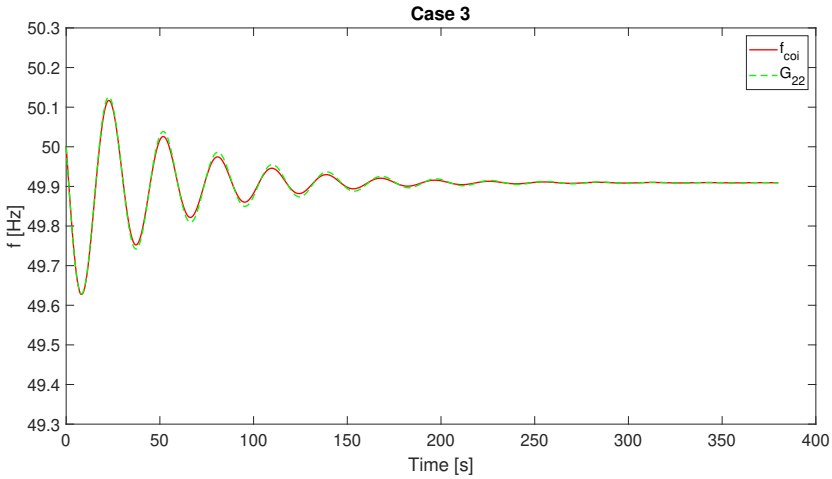

Figure 5.2: Tuning of $G_2(s)$ based on case 3 illustrating how both the frequency drop and the ensuing system oscillations could be captured by tuning the transfer function.

The largest difference in tuning seemed to manifest in the system inertia H and gain K variables. Both of the adjustable time constants T_1 and T_2 ended up in the area around 0.4 and 16.1 respectively, with differences of only around 0.1 or less in both cases. Contrarily the variables in system inertia and gain were much larger, over total ranges of 0.5 and 0.66 respectively. Both of these parameters are properties of an electrical power system that TSOs may have accurate data and numbers for. The total effective inertia, and the expected RoCoF following disturbances, can either be calculated from rated system values or estimated from the dynamics of frequency measurements. As an example, a method for online estemation of system inertia was implemented as a test project on iceland in [8], which could be used together with the prediction methods in this thesis.

5.3 Predictions

It can finally be noted that the the oscillations of the system were well captured by the $G_2(s)$ transfer function predictions. The swing time seem to well tuned in line with the actual response of the system. It is clear from the long term plots that the damping in most cases in larger for the system than the predictive cases. On the contrary, G_1 does not encapsulate the oscillations and the general time swing time of the system for an of the cases. Its oscillations are swinging too fast and is damped out to quick. This is in line with the expectations, as it is a less complex model with more simplifications.

The predictions were able to predict the the general development of the tested cases, and with high accuracy when the initial RoCoF was accurately predicted. When initial RoCoF was not correctly predicted, the absolute errors became much larger. This can be exemplified for the predictions of case 8, by comparing the case 1 and case 4 predictions. The two tuning approaches had a large deviation in system inertia which resulted in different predictions for the inital RoCoF. Predictions based on case 4 tuning were much closer than the ones from case 1. This is illustrated in figure 5.3.

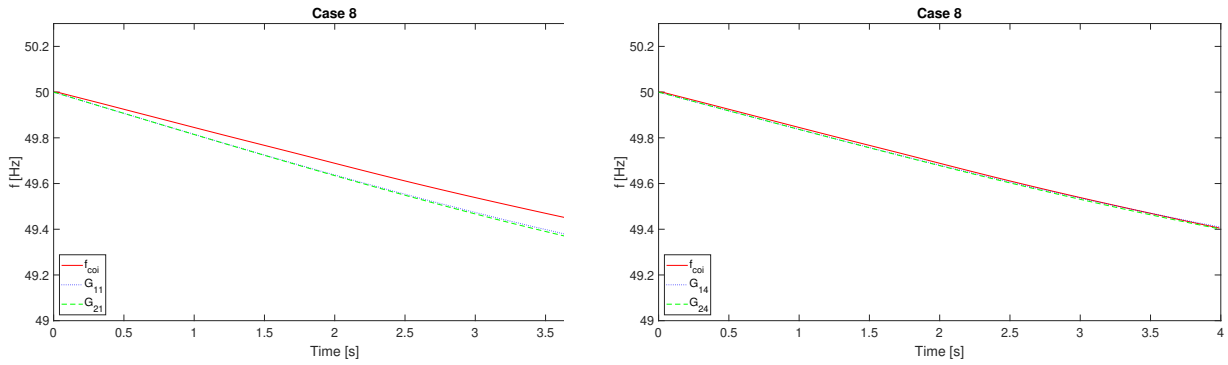

(a) Case 1 tuning

(b) Case 4 tuning

Figure 5.3

This dynamic resulted in case 1 and case 2 predicting cases 6 and 7 well, which had a steeper initial frequency drop. Meanwhile case 3 and case 4 with larger system inertia constant was able to predict cases 5 and 8 better, cases that had lower initial RoCoF.

The error margins were in total very varying, ranging from close to insignificant (3-5 mHz) to more substantial sizes (100 mHz). Frequency-measurements used for FCR purposes are required to have an accuracy of 0.01 % (5 mHz)[28], and prediction errors under this size are therefore considered negligible. An absolute error of 103 mHz, which is the largest occuring prediction error, is more significant. The operational range which is considered standard by Statnet is 49.9-50.1 Hz. For disturbances, the goal of frequency control is to limit any deviations to stay above 49.0 Hz [6]. The FCR-D generator reserves start activating at 49.9 Hz and is fully activated at 49.5 Hz [12]. In total, this means that activation of primary reserves occur over the range of 0.4 Hz, and the total allowable frequency

range is 0.9 Hz. The maximum frequency prediction error was 103 mHz which corresponds to 26 % of the FCR-D activation range, and 11.4 % of the fault containment range.

The mean absolute error was 40 mHz, and the two transfer functions performed practially identical. This is larger than other approaches using regressional analysis in [2] to calculate maximum frequency deviations. The results here gave mean absolute errors in the range between 18-36 mHz. It is possible that the absolute error would be smaller than this range if the inertia variable corresponded better with the initial RoCoF of the prediction test cases.

Time deviations were generally small, and in the sense of frequency control can be considered negligible. Both prediction models had time deviations typically in the area of at most 0.25 s. As seen from the simulations, the frequency drop takes around 8 seconds to reach its nadir. Even FFR activation time limits are almost an order of magnitude larger than this [29]. To put it into perspective, the largest RoCoF caulated from f_{coi} is 0.16 Hz/s. So a time deviation of 0.25 would at the worst case scenario immediately after a disturbance correspond to 0.04 Hz. Since the RoCoF is also zero at the nadir, the time deviation of 0.24 seconds and below is negligible when considering the general development of a frequency disturbance.

The reader should note that from the small set of test and tune cases the statistical measurements are highly inconclusive, since the test set is so small.

5.4 Real generator trip

It should be noted that the system oscillation occurring for several minutes throughout the simulations are not typical for the real Nordic interconnected system. Oscillations typically die out after the first couple of swings. This is exemplified in figure 5.4, where a real frequency measurement has been made at Hasle, following an outage of a nuclear generator at Olkiluoto, Finland[30]. This specific generator trip was connected to a pilot test of Fast Frequency Response (FFR) units. The FFR-units can be seen as the notches in the slope around 2 and 15 seconds, respectively indicating the point of activation and deactivation of the FFR power provision.

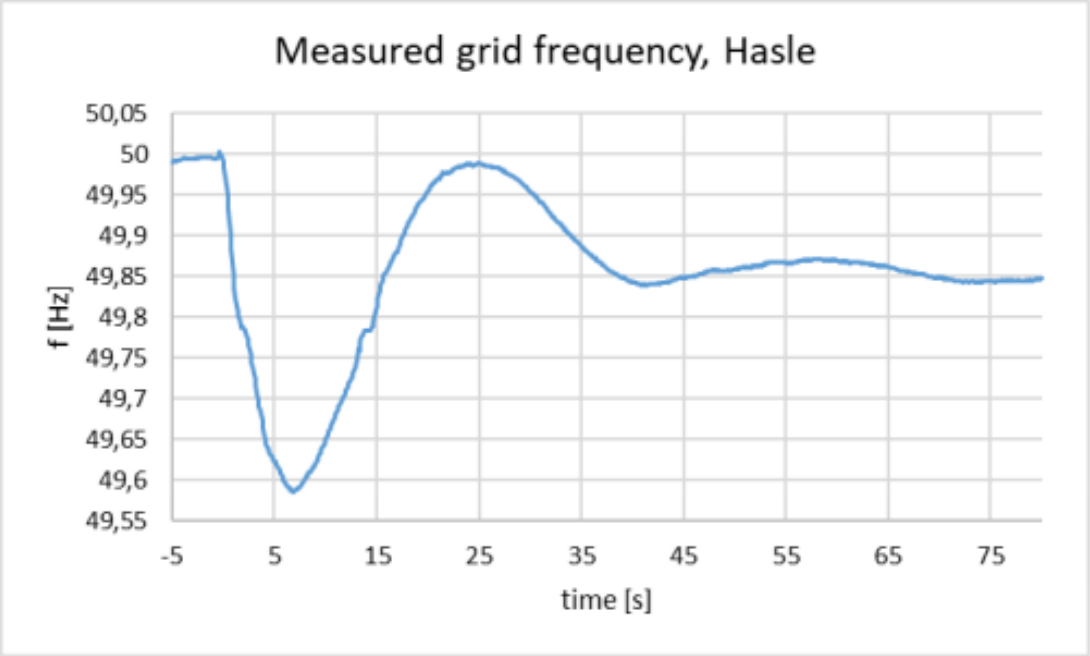

Figure 5.4: Measured frequency at Hasle, for a generator trip of 880 MW at Olkiluoto 2, in Finland. In the N44 model, this measurement corresponds to a frequency measurement from bus 5101, and the generator trip would correspond to a trip of the second generator connected to bus 7000.

Chapter 6

Conclusion and further work

6.1 Conclusion

A version of the Nordic synchronous system was represented by the Nordic 44 bus system in PSSE. This model was ran in the real time online simulator ePHASORSIM and attempts were made at predicting the frequency drop following large generator outages, based on the loss of their delivered active power. The turbine speed deviation of 48 generators were recorded in the simulations and aggregated into a center of inertia frequency. Two transfer function prediction models based on the HYGOV turbine governor were used to aggregate the system response into two transfer function models. These transfer functions had their variables tuned based on 4 simulated cases such that the initial frequency drop of the system fit with their respective step responses. Loss of active power was used as step input. Then 4 new test cases were ran, and their respective time responses of system frequency were attempted predicted.

The frequency drop was predicted with an mean absolute error of 40 mHz and a mean absolute time deviation of 0.2 s. The accuracy of the frequency drop estimation was highly varying and dependent on the inertia estimation from the tuning process. It is believed that the accuracy of predictions would improve given an inertia estimation process based on the initial rate of change of frequency of the case being predicted. Time deviation was satisfactory, and are believed to be within reasonable limits of what transmission system operators would expect.

6.2 Further work

A suggestion of further work is to test the system for different cases of effective inertia. Much work has been made on evaluating the development of the system inertia of the Nordic synchronous system [2] [31] [7]. Other operational situations could be considered for example based on the forecasts for 2025.

Bibliography

[1] Amund Kulsrud Storruste. *Real-time simulations of the Nordic electrical transmission system for development of WAMS applications*. Specialization project. Norwegian University of Science and Technology, Feb. 2020.

[2] entsoe. *Future system inertia*. Tech. rep. 2015. URL: https://www.statnett.no/globalassets/for-aktorer-i-kraftsystemet/utvikling-av-kraftsystemet/nordisk-frekvensstabilitet/future-system-inertia-phase-1.pdf.

[3] Energinet et al. *A Survey on Inertia Related Challenges and Mitigation Measures*. Tech. rep. URL: https://www.statnett.no/globalassets/for-aktorer-i-kraftsystemet/utvikling-av-kraftsystemet/nordisk-frekvensstabilitet/nordic-tsos-survey-on-inertia-related-challenges-and-mitigation-measures.pdf.

[4] *Ny beregning av aktivert FCR*. Statnett. June 2019. URL: https://www.statnett.no/globalassets/for-aktorer-i-kraftsystemet/marked/reservemarkeder/ny-beregning-av-aktivert-fcr.pdf (visited on 08/11/2020).

[5] Jan Machowski. *Power system dynamics : stability and control*. eng. Chichester, 2008.

[6] entsoe. *FCR-D design of requirements – phase 1*. Tech. rep. 2017. URL: https://www.statnett.no/globalassets/for-aktorer-i-kraftsystemet/utvikling-av-kraftsystemet/nordisk-frekvensstabilitet/fcr-d-design-of-requirements.pdf.

[7] entsoe. *Fast Frequency Reserve – Solution to the Nordic inertia challenge*. Tech. rep. Dec. 2019. URL: https://www.statnett.no/globalassets/for-aktorer-i-kraftsystemet/utvikling-av-kraftsystemet/nordisk-frekvensstabilitet/ffr-stakeholder-report_13122019.pdf.

[8] K. Tuttelberg et al. "Estimation of Power System Inertia From Ambient Wide Area Measurements". In: *IEEE Transactions on Power Systems* 33.6 (Nov. 2018), pp. 7249–7257. ISSN: 1558-0679. DOI: 10.1109/TPWRS.2018.2843381.

[9] Robert Eriksson, Niklas Modig, and Katherine Elkington. "Synthetic inertia versus fast frequency response: a definition". In: *IET Renewable Power Generation* 12 (Sept. 2017). DOI: 10.1049/iet-rpg.2017.0370.

[10] *Weighted arithmetic mean*. Wikpedia. 2020. URL: https://en.wikipedia.org/wiki/Weighted_arithmetic_mean (visited on 08/04/2020).

[11] A. K. Storruste and O. M. Forbord. *A Brief Introduction to Synthetic Inertia and Control Mechanisms for Provision of Frequency Support in Wind Power Systems*. eng. 2019.

[12] Statnett. *Vilkår for tilbud, aksept, rapportering og avregning i marked for FCR*. 2019.

[13] Katrine Gabrielsen Andersen. *Area Based Secondary Frequency Control in the Nordic Power System*. eng. 2016. URL: http://hdl.handle.net/11250/2408871.

[14] Jens G Balchen. *Reguleringsteknikk*. nob. Trondheim, 2003.

[15] "Hydraulic turbine and turbine control models for system dynamic studies". In: *IEEE Transactions on Power Systems* 7.1 (1992), pp. 167–179.

[16] D. P. Kothari and I. J. Nagrath. *Electric Machines, 5/e*. eng. 2008.

[17] *Model Library PSSE 34.5.1*. 2018.

[18] Wikipedia contributors. *Final value theorem — Wikipedia, The Free Encyclopedia*. [Online; accessed 4-August-2020]. 2020. URL: https://en.wikipedia.org/w/index.php?title=Final_value_theorem&oldid=967153800.

[19] *De systemansvarlige nettselskapene i Norden har inngått ny systemdriftavtale*. Statnett. 2020. URL: https://www.statnett.no/om-statnett/nyheter-og-pressemeldinger/nyhetsarkiv-2019/de-systemansvarlige-nettselskapene-i-norden-har-inngatt-ny-systemdriftsavtale/ (visited on 01/29/2020).

[20] Sigurd Jakobsen and Espen Solvang. *The Nordic 44 test network*. Tech. rep. Dec. 2018. DOI: 10.6084/m9.figshare.7464386.v1.

[21] Dinh Thuc Duong. *Online Voltage Stability Monitoring and Coordinated Secondary Voltage Control*. eng. 2016. URL: http://hdl.handle.net/11250/2410911.

[22] *Real-Time Simulation of Over 100,000 NOdes of T and D Systems*. OPAL-RT. 2019. URL: https://blob.opal-rt.com/medias/L00161_0775.pdf (visited on 01/29/2020).

[23] *Download PDF maps*. entsoe. 2020. URL: https://www.entsoe.eu/data/map/downloads/ (visited on 01/30/2020).

[24] *Øvre Røssåga vankkraftverk*. Statkraft. 2020. URL: https://www.statkraft.no/om-statkraft/hvor-vi-har-virksomhet/norge/ovre-rossaga-vannkraftverk/.

[25] *Nedre Røssåga vankkraftverk*. Statkraft. 2020. URL: https://www.statkraft.no/om-statkraft/hvor-vi-har-virksomhet/norge/nedre-rossaga-vannkraftverk/.

[26] entsoe. *FCR-D design of requirements – phase 2*. Tech. rep. 2019. URL: https://www.statnett.no/globalassets/for-aktorer-i-kraftsystemet/utvikling-av-kraftsystemet/nordisk-frekvensstabilitet/fcr-d-design-of-requirements--phase-2.pdf.

[27] S. Azizi et al. "Local Frequency-Based Estimation of the Rate of Change of Frequency of the Center of Inertia". In: *IEEE Transactions on Power Systems* (2020), pp. 1–1.

[28] Statnett. *Funksjonskrav i kraftsystemet 2012*. Tech. rep. Husebybakken 28b, 2020. URL: https://www.statnett.no/om-statnett/nyheter-og-pressemeldinger/Nyhetsarkiv-2012/funksjonskrav-i-kraftsystemet-fiks-2012-publisert-/ (visited on 01/22/2020).

[29] Statnett. *FFR-demo 2020, betingelser for deltagelse i demonstrasjonsprosjekt*. Tech. rep. Feb. 2020. URL: https://www.statnett.no/globalassets/for-aktorer-i-kraftsystemet/utvikling-av-kraftsystemet/nordisk-frekvensstabilitet/ffr-demo-2020/ffr-demo-2020-betingelser-for-deltagelse-i-demonstrasjonsprosjekt.pdf.

[30] Statnett. *Fast Frequency Reserves 2018 - Pilot for raske frekvensreserver*. 2018.

[31] entsoe. *Future system inertia 2*. Tech. rep. 2017. URL: https://www.statnett.no/globalassets/for-aktorer-i-kraftsystemet/utvikling-av-kraftsystemet/nordisk-frekvensstabilitet/future-system-inertia-phase-2.pdf.

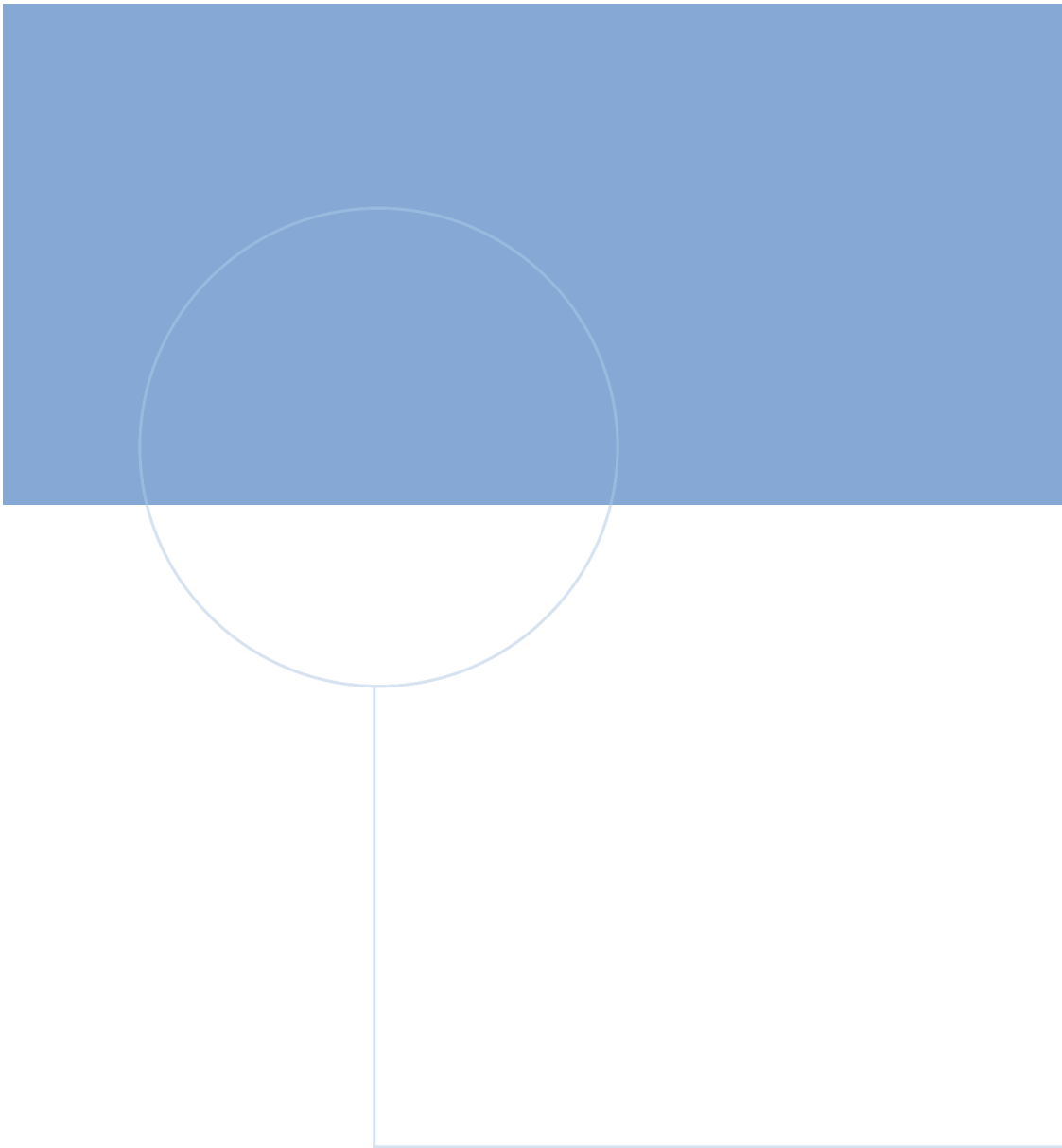

NTNU

Kunnskap for en bedre verden